doi:10.1093/plphys/kiab339 PLANT PHYSIOLOGY 2021: 187: 550–571

Plant Physiology®

Update

Illuminating the hidden world of calcium ions in plants with a universe of indicators

Matteo Grenzi ,[1] Francesca Resentini ,[1] Steffen Vanneste ,[2,3,4] Michela Zottini ,[5] Andrea Bassi [6,7] and Alex Costa [1,8,*,†]

1 Department of Biosciences, University of Milan, 20133 Milano, Italy
2 Department of Plant Biotechnology and Bioinformatics, Ghent University, 9052 Ghent, Belgium
3 Department of Plants and Crops, Ghent University, 9000 Ghent, Belgium
4 Laboratory of Plant Growth Analysis, Ghent University Global Campus, Incheon 21985, South Korea
5 Department of Biology, University of Padova, 35131 Padova, Italy
6 Department of Physics, Politecnico di Milano, 20133 Milano, Italy
7 Institute of Photonics and Nanotechnologies, National Research Council of Italy (CNR), 20133 Milano, Italy
8 Institute of Biophysics, National Research Council of Italy (CNR), 20133 Milano, Italy

*Author for communication: alex.costa@unimi.it
†Senior author

M.G. carried out the experiments reported in Figures 3 and 4 and prepared Figures 1, 3, and 4. F.R. prepared Tables 1 and 4. A.C. conceived the project and wrote the article with feedback from all authors. A.C. serves as the author responsible for contact and ensures communication.
The author responsible for distribution of materials integral to the findings presented in this article in accordance with the policy described in the Instructions for Authors (https://academic.oup.com/plphys/pages/General-Instructions) is Alex Costa (alex.costa@unimi.it).

Introduction

Calcium (Ca^{2+}) is a well-known second messenger in both unicellular and multicellular organisms (Berridge et al., 2000; Carafoli and Krebs, 2016). In plants, apart from its role as a structural component (White and Broadley, 2003), calcium plays a role in signaling events in response to a multitude of developmental and environmental stimuli (Kudla et al., 2010; Edel et al., 2017; Kudla et al., 2018). Biotic and abiotic challenges affect the cellular Ca^{2+} homeostasis by triggering transient changes of Ca^{2+} concentrations in the cytosol as well as in subcellular compartments (McAinsh and Pittman, 2009; Stael et al., 2012; Costa et al., 2018; Pirayesh et al., 2021; Resentini et al., 2021b).

The basis of calcium's role as a signaling component lies in its peculiar chemistry and the existence of a large electrochemical gradient across the cell's membranes, maintained by the activity of the proton- and calcium-ATPases (H^+-ATPases and Ca^{2+}-ATPases; Palmgren, 2001; Demidchik et al., 2018; Klejchova et al., 2021). The main evolutionary reason for evolving mechanisms that generate and maintain this large gradient is based on the need to keep the cytosolic Ca^{2+} concentrations ($[Ca^{2+}]_{cyt}$) low, to prevent the precipitation of organic and inorganic molecules (e.g.

ADVANCES

- GECIs have been efficiently employed in plants.
- In vivo Ca^{2+} imaging at high spatial and temporal resolution is possible at tissue, cell, and organelle levels.
- Plants expressing GECIs with different affinities for Ca^{2+} are available for cytosolic and organellar analyses.
- Ratiometric GECIs allow a reliable comparison of Ca^{2+} levels in different genetic backgrounds and in long-term treatments.
- Intensiometric GECIs require simple and cost-effective imaging setups.

Received February 23, 2021. Accepted July 15, 2021

phosphates including adenosine triphosphate (ATP)) (Clapham, 2007). Under resting conditions, the $[Ca^{2+}]_{cyt}$ is in the range of hundreds of nanomolar (100–200 nM) whereas in the external spaces and subcellular compartments it can reach up to millimolar ranges (Stael et al., 2012). This steep concentration gradient implies that the opening of a limited number of calcium permeable channels, located on the different cellular membranes, is sufficient to rapidly increase the $[Ca^{2+}]_{cyt}$ with a 10-fold increase compared with the resting concentration (Demidchik et al., 2018).

Within the plant cell, the change in $[Ca^{2+}]_{cyt}$ is sensed by Ca^{2+} binding proteins acting as primary responders (e.g. calcium dependent kinases) or sensor relays. Among the latter Calmodulin (CaM), CaM-like proteins (CMLs) and calcineurin B-like proteins (CBLs) all bind cytosolic calcium, which triggers a conformational change of the proteins enabling them to interact with different targets modulating their activities (Kudla et al., 2018; Tian et al., 2020). When the Ca^{2+} sensors are stimulated they become primed to regulate downstream processes, which include ion fluxes, enzymatic activities, transcription, etc. (DeFalco et al., 2010; Kudla et al., 2018; Tian et al., 2020). Importantly, after the perception of a stimulus and the occurrence of the Ca^{2+} transient, resting $[Ca^{2+}]_{cyt}$ needs to be quickly reestablished to prevent cell death (Clapham, 2007). The molecular mechanisms that are responsible for the recovery of the resting $[Ca^{2+}]_{cyt}$ are Ca^{2+} buffers and Ca^{2+} active transporters, such as Ca^{2+}-ATPases and Ca^{2+}/cation exchangers (CAX) that are localized in the plasma membrane and membranes of intracellular compartments (Corso et al., 2018; Costa et al., 2018; Demidchik et al., 2018; Hilleary et al., 2020; Ishka et al., 2021; Resentini et al., 2021b).

The intertwined and coordinated activities of influx and efflux Ca^{2+} transport systems in the plasma membrane and internal stores (Stael et al., 2012; Costa et al., 2018; Pirayesh et al., 2021; Resentini et al., 2021b) jointly shape the characteristic cellular Ca^{2+} dynamics, also called Ca^{2+} signatures (Sanders et al., 2002).

The possibility of visualizing and studying Ca^{2+} signatures is based on the exploitation of "calcium imaging techniques" that, thanks to continuous improvement, have allowed us to study Ca^{2+} dynamics with increasing resolution and sensitivity with minimal invasiveness in different organisms, including plants. An important boost for the progression of the calcium imaging techniques is the possibility to extend the use of valuable and innovative tools across the different kingdoms of life. In such a scenario, one driver of innovation is neuroscience studies. In neurons, action potentials (APs) or the activation of ionotropic glutamate receptors trigger large and rapid changes in $[Ca^{2+}]_{cyt}$ (Tian et al., 2009). This has led neuroscientists to develop innovative technologies to study Ca^{2+} dynamics, which are historically based on the simultaneous and continuous improvement of Ca^{2+} indicators, and the development and the implementation of the appropriate microscopy instrumentation.

In this update, we will briefly retrace the history of Ca^{2+} sensitive indicators (Fig. 1) focusing on their use in plants, providing important clues about how to choose among them, and also taking into consideration the most appropriate imaging techniques. We will explain when it is recommended to use ratiometric biosensors and when instead it is reasonable and more convenient to use intensiometric ones. The intention of this update is to guide the readers into the recent developments in the area of Ca^{2+} biosensing in plants and make them enthusiastic about this amazing and imaginative field of research.

Synthetic dyes for measurements of cytosolic calcium dynamics

A breakthrough in the field of Ca^{2+} imaging was the development of sensitive fluorescent Ca^{2+} indicators (or dyes) and buffers by Tsien (1980). These indicators were the result of the "fusion" between Ca^{2+}-selective chelators like ethylene glycol-bis(β-aminoethyl ether)-*N*,*N*,*N*′,*N*′-tetraacetic acid (EGTA) or 1,2-bis(o-aminophenoxy)ethane-*N*,*N*,*N*′,*N*′-tetraacetic acid (BAPTA) with a fluorescent chromophore (Fig. 2).

In plants, the first attempts to study Ca^{2+} dynamics in vivo were based on the use of Ca^{2+} sensitive dyes (e.g. Fura-2, Fura-2 dextran, calcium green dextran, and Indo-1) which were instrumental in measuring $[Ca^{2+}]$ in aleurone protoplasts, guard cells in response to ABA, in growing pollen tubes or in root hairs in response to nodulation factors (Bush and Jones, 1987; McAinsh et al., 1990; Gilroy et al., 1991; McAinsh et al., 1995; Ehrhardt et al., 1996; Holdaway-Clarke et al., 1997). The use of those dyes allowed the measurement, for the first time, of Ca^{2+} variation within isolated mitochondria from land plants, giving the basic knowledge of the molecular mechanism for Ca^{2+} uptake in these organelles (Zottini and Zannoni, 1993). Whereas the use of Ca^{2+}-sensitive dyes allowed the making of fundamental discoveries, they have some limitations which primarily include (i) their requirement to be loaded or manually injected into the cells, possibly leading to an unequal amount of dye within different cells; (ii) when accumulated into the cells they can be compartmentalized or sequestered into vacuoles (Bush and Jones, 1990); and (iii) an excessive loading can affect cytosolic Ca^{2+} availability due to their Ca^{2+} chelator-backbone (Bush and Jones, 1990; Table 1). Nevertheless, a major advantage of Ca^{2+}-sensitive dyes is the ability to perform Ca^{2+} imaging analyses without the need to generate transgenic plants (see the next section), as transformation protocols are not available for every species (Table 1). If a reliable Ca^{2+}-sensitive dye for plant cells were to be available, it could be used for example to perform the first screen of

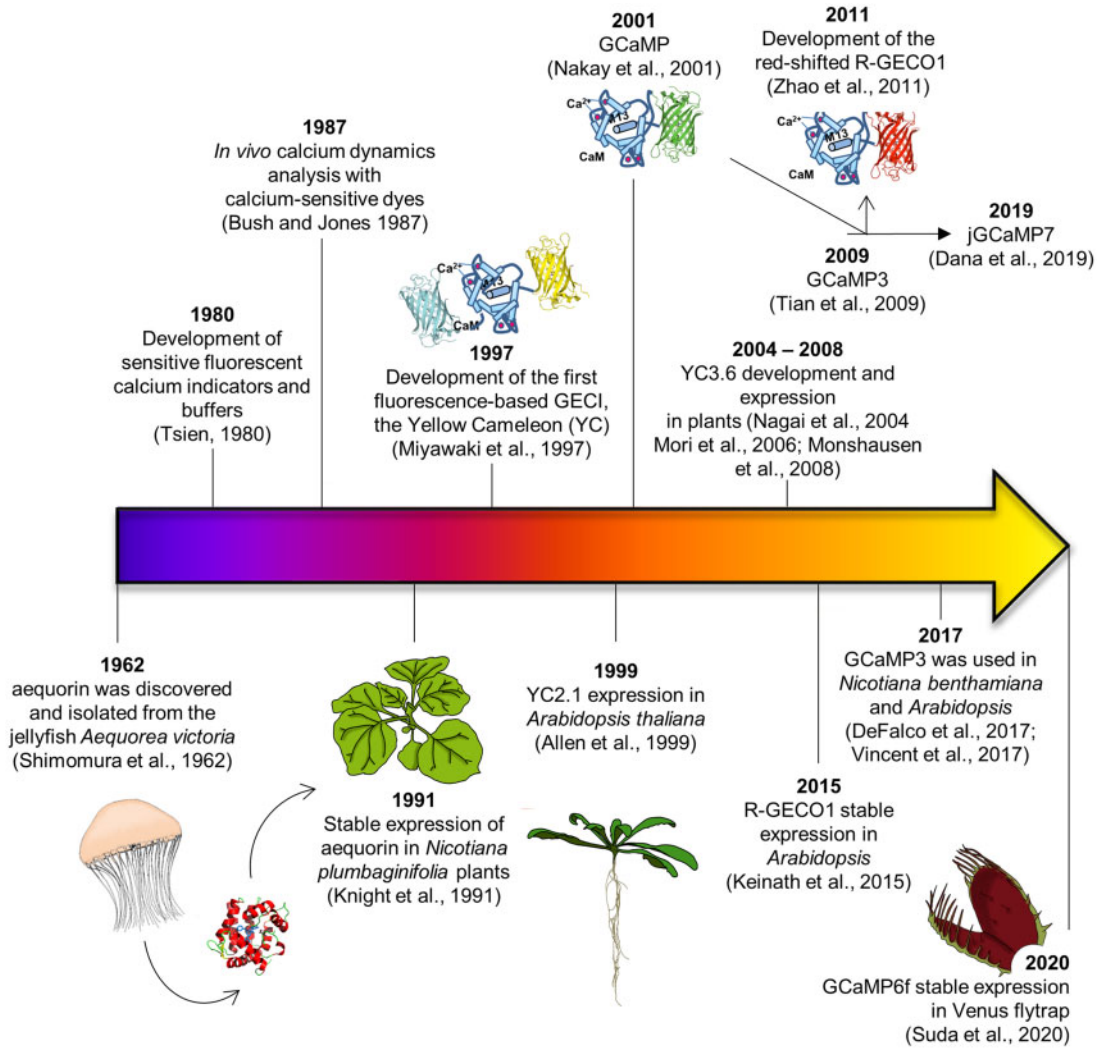

Figure 1 History of major achievements for the in vivo study of Ca^{2+} biosensing in plants.

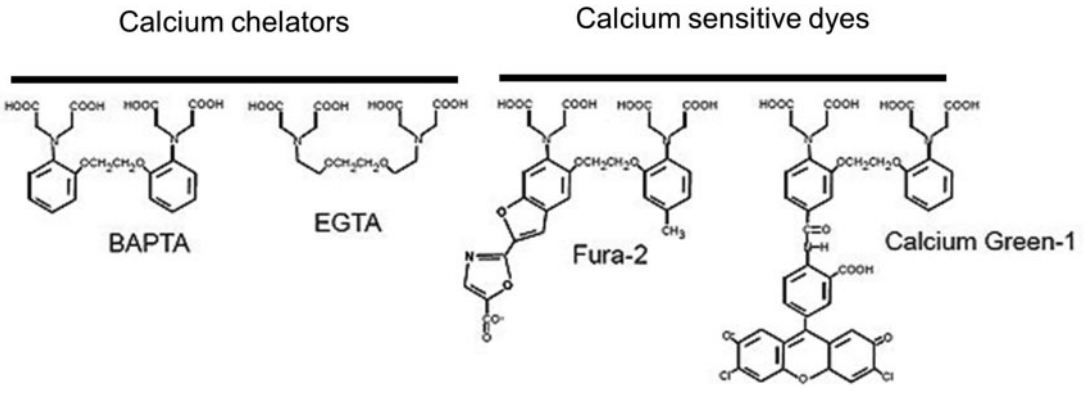

Figure 2 Examples of two commonly used Ca^{2+} chelators and calcium-sensitive dyes derived from them.

mutants, instead of performing a tedious transgenic plants selection (Fichman and Mittler, 2021). Nevertheless, since the use of dyes has still more disadvantages than advantages, in the last 20 years, plant scientists have moved to the use of genetically encoded Ca^{2+} indicators (GECIs) (Perez Koldenkova and Nagai, 2013) which opened

Table 1 Summary of advantages and disadvantages/limitations of the different available Ca^{2+} indicators

Type of indicator	Advantages	Disadvantages/limitations
Synthetic dyes	(i) Ca^{2+} imaging analyses without the need to generate transgenic plants.	(i) To be loaded or manually injected into the cells; (ii) can be compartmentalized or sequestered into vacuoles; (iii) an excessive loading can bring to cytosolic Ca^{2+} buffering.
Aequorin	(i) Does not need to be excited with fluorescent light; (ii) long-term experiments; and (iii) it allows a good estimation of Ca^{2+} concentrations.	(i) Low quantum yield efficiency; (ii) requirement for the external provision of coelenterazine; and (iii) non-linearity of its rate of light emission.
Ratiometric GECIs (e.g. Cameleon, YC-Nano)	(i) Reliability; (ii) reduced artifacts; (iii) strong independence from the expression levels; and (iv) good for genetic backgrounds comparison of resting Ca^{2+}.	(i) Large size of the indicators; (ii) tailored strategies for their targeting; (iii) possible silencing issues; and (iv) more sophisticated and expensive imaging equipment is required.
Intensiometric GECIs (e.g. GECOs/ GCaMPs)	(i) Need simple microscope setups; (ii) sensitivity to detect subtle changes of Ca^{2+}; (iii) they allow the easy measurement of Ca^{2+} in adult plants; and (iv) an easier combination of different spectral variants for simultaneous imaging of Ca^{2+} in different compartments.	(i) Possible artifacts related to their intensiometric nature and (ii) Ca^{2+} buffering with some high affinity and high Hill coefficient variants.

another dimension for the quantitative in vivo imaging of Ca^{2+} dynamics.

Genetically encoded calcium indicators

Aequorin

Aequorin is a bioluminescent protein that was discovered and isolated from the jellyfish *Aequorea victoria* by Shimomura et al. (1962). Shimamura was awarded the Nobel Prize in 2008 together with Martin Chalfie and Roger Tsien for the discovery and exploitation of the green fluorescent protein (GFP). Without the work done by these three visionary scientists this Update, this Focus Issue, and a large field of bio-imaging would not exist.

Aequorin is a 22-kDa holoprotein that contains bound oxygen, a prosthetic group, the coelenterazine, and three Ca^{2+}-binding sites. When aequorin binds Ca^{2+} ions (Shimomura, 1995), it undergoes a conformational change, converting itself into a luciferase, which then catalyzes the luminescence reaction of coelenterazine. Coelenterazine is oxidized to coelenteramide with the emission of CO_2 and blue light (at 465 nm) which is caused by the decay of the coelenteramide from an excited state (Ohmiya and Hirano, 1996). This property offered a useful tool for detecting the concentration of Ca^{2+} ions in real time. However, the aequorin quantum yield is very low, requiring the simultaneous reactions of hundreds or thousands of proteins to collect enough photons to a level detectable by photon emission measurements (Mithöfer and Mazars, 2002). Nevertheless, identification of the aequorin gene and of its coding sequence (Prasher et al., 1985) allowed the protein to be expressed recombinantly in cells and tissues from different organisms. In the 1980s, the injection of recombinant aequorin in Chara allowed the detection of a transient increase in light emission when the cell generated an AP (Williamson and Ashley, 1982). A real revolution then occurred in 1991 when Marc Knight and colleagues generated the very first transgenic multicellular organism, *Nicotiana plumbaginifolia* plants, stably expressing aequorin (Knight et al., 1991; Figure 1). The authors reported that in response to touch, cold-shock, and elicitors, the plants showed clear photon emission determined by cytosolic Ca^{2+} increase. This demonstration opened de facto the modern *era* of Ca^{2+} imaging in plants. Indeed, the low quantum yield of aequorin hinders high-resolution imaging and, as a matter of fact, its detection was usually carried out with the use of a luminometer, collecting the emitted photons without creating an image (Mithöfer and Mazars, 2002). However, modern ultrasensitive cameras now allow the detecting of the photons emitted by a single whole plant, providing low-resolution images and averaged responses from different tissues or cells (Kiegle et al., 2000; Zhu et al., 2013; Kiep et al., 2015). Therefore, the recent technological advances in camera sensitivity have revitalized the use of aequorin imaging, posing the basis for the design of powerful and successful genetic screenings (Yuan et al., 2014; Jiang et al., 2019; Chen et al., 2020; Wu et al., 2020).

Even if aequorin is the oldest GECI, it still represents a reliable tool to study Ca^{2+} dynamics in plants, in particular, to determine quantitatively the magnitude of the responses. In fact, for every single experiment, the measurement of the light expressed as relative luminescence units (RLUs) can be converted into absolute $[Ca^{2+}]$ thanks to a calibration curve that considers the total amount of aequorin molecules present in the sample. This can be done by discharging the reconstituted aequorin with a solution containing Ca^{2+} and ethanol (100 mM $CaCl_2$, 10% ethanol (v/v)) (Allen et al., 1977; Mithöfer and Mazars, 2002). Specifically, the formula used to perform the conversion is the one reported in Mithöfer and Mazars (2002):

$$[Ca^{2+}] = \{(L_0/L_{max})^{1/3} + [KTR(L_0/L_{max})^{1/3}]-1\}/\{KR-[KR(L_0/L_{max})^{1/3}]\},$$

where L_0 is the aequorin luminescence intensity per second and L_{max} is the total amount of luminescence present in the sample over the experiment. KR and KTR are the dissociation constants for the first and second Ca^{2+} ions bound by aequorin, respectively (Mithöfer and Mazars, 2002).

As with every technique, aequorin-based Ca^{2+} analysis presents both advantages and disadvantages (Table 1). An

advantage of aequorin is that it does not need to be excited with fluorescent light, which helps when the measurement of Ca^{2+} levels for long time intervals is required (Sai and Johnson, 2002; Love et al., 2004; Martí et al., 2013; Martí Ruiz et al., 2020) . Among the disadvantages, besides the already cited low quantum yield efficiency, is its requirement for the external provision of coelenterazine (Knight et al., 1991; Mithöfer and Mazars, 2002) which foresees the incubation of the plant material with the prosthetic group for several hours before starting the experiment. Moreover, after its oxidation, coelenterazine is irreversibly consumed, with the consequent decrease of the active aequorin pool. Another disadvantage of aequorin is the non-linearity of light emission rate as a function of the Ca^{2+} concentration (Robert et al., 2000; Table 1). Within the physiological range of $[Ca^{2+}]_{cyt}$ (10^{-7}–10^{-5} M), the photon emission rate increases by more than 100-fold for a 10-fold change in $[Ca^{2+}]$. In practical terms, this means that for a change in $[Ca^{2+}]$ from 0.1 μM (at resting) to 3–4 μM (in response to a stimulus), the rate of aequorin photon emission increases over 1000-fold. As a consequence, the signal coming from 1 activated cell will be the same as that of 1000 cells at resting $[Ca^{2+}]$. If Ca^{2+} is not homogeneous in the population of cells, which is indeed the case when using entire seedlings or leaf disks, the overall aequorin light emission is dominated by the most responding cells subpopulation, leading to an averaging of the response. One way that can be followed to study more specifically the contribution of different cell types is the expression of aequorin under the control of tissue-specific promoters or using enhancer trap lines. By following this strategy, it was possible to discover the oscillatory dynamics of Ca^{2+} signaling in root cells (Kiegle et al., 2000), circadian gating of cold-induced Ca^{2+} oscillations in guard cells (Dodd et al., 2006), and cell-type and stimulus-specific Ca^{2+} oscillations (Martí et al., 2013).

Aequorin being a GECI could also be targeted to different subcellular compartments, such as the tonoplast (Knight et al., 1996), the nucleus (van Der Luit et al., 1999), the Golgi apparatus (Ordenes et al., 2012), mitochondria (Logan and Knight, 2003), plastids/chloroplasts (Johnson et al., 1995; Mehlmer et al., 2012; Sello et al., 2016), chloroplast subcompartments like the outer and inner envelope membranes (Mehlmer et al., 2012), and the thylakoid lumen and membrane (Sello et al., 2018; Table 2). Aequorin was also targeted to the apoplastic space (Gao et al., 2004).

In *A. victoria*, the photons emitted by aequorin excite the GFP which causes the jellyfish to emit fluorescence (Prasher et al., 1992). In laboratory experiments, this property has been exploited to generate a bioluminescence resonance energy transfer (BRET)-based GFP-aequorin reporter (i.e. G5A; Baubet et al., 2000; Rogers et al., 2005). This BRET-based sensor has overcome one of the major limitations of aequorin, that is its low amount of emitted light. This allows easier detection of $[Ca^{2+}]$ variations using a camera by permitting the possibility to reduce the exposure time compared with aequorin imaging. However, this sensor still requires the exogenous administration of coelenterazine. Nevertheless, the G5A sensor expression in Arabidopsis (*Arabidopsis thaliana*) plants by Xiong et al. (2014) allowed visualization for the first time of long-distance Ca^{2+} waves propagating from the roots to shoot upon salt treatment.

FRET-based fluorescent sensors

To overcome aequorin limitations, in the late 1990s, scientists started to exploit fluorescent proteins (FPs) (i.e. GFP) and its spectral variants to develop another generation of GECIs. The first ever fluorescence-based GECI, named Yellow Cameleon (YC), was developed by Roger Tsien in 1997 (Miyawaki et al., 1997) quickly followed by the development of the YC2.1 version (Miyawaki et al., 1999) which was shortly after expressed in plants (Allen et al., 1999; Figure 1). This sensor is based on the Ca^{2+}-induced protein–protein interaction between CaM and the CaM-binding peptide M13, a fragment from the myosin light chain kinase (Miyawaki et al., 1997). Both components are fused by a flexible linker and are sandwiched between a FP pair with partial overlap between the emission spectrum of the donor and the absorption spectrum of the acceptor. Upon Ca^{2+} binding, CaM interacts with M13, bringing the donor and acceptor FPs into sufficiently close proximity to allow for Förster resonance energy transfer (FRET) between them through a nonradiative dipole–dipole coupling. This phenomenon can be measured via fluorescence microscopy. At the level of the acceptor molecule, it results in the emission of fluorescence upon excitation of the donor, allowing the estimation of Ca^{2+}-induced FRET by the ratio of donor and acceptor emission upon excitation of the donor using relatively simple microscopy setups (Miyawaki et al., 1997; Rudolf et al., 2003).

A wide variety of FRET-based GECI has been developed based on FRET pairs with different spectral properties and in combination with a variety of Ca^{2+} regulated protein–protein interactions (Greenwald et al., 2018; https://biosensordb.ucsd.edu/biosensorDB/bsSearch.php). The spectral range of the FRET pairs is usually cyan/yellow, green/red occupying a wide spectrum, reducing the options for dual imaging with other sensors or reporters.

In plants, the most popular FRET-based GECIs are based on cyan and yellow FRET pairs linked together by the Ca^{2+}-binding protein CaM and the CaM-binding peptide M13, as in the original YC configuration by Roger Tsien. FRET, and thus $[Ca^{2+}]$ increases, can be conveniently measured by the increase in the ratio between the emission intensity of Enhanced Yellow FP (EYFP) and Enhanced Cyan FP (ECFP) upon ECFP excitation. The Cameleon indicators can go back and forth from the bound and unbound Ca^{2+} state. However, this is limited by the bleaching of the sensor by the excitation light especially when high magnifications are used, which may cause photo-oxidative cellular stress (Laissue et al., 2017). One of the most important properties of Cameleon is its pure ratiometric nature: a single wavelength excitation and a dual emission (Miyawaki et al., 1997). The advantages of having a ratiometric sensor will be further discussed in the next section. The Cameleon's

Table 2 Summary of available fluorescent-based GECIs used in plants

Name	Version	Type	Peaks of excitation/emission (nm)	In vitro K_d for Ca^{2+a}	Subcellular localization	References
Cameleon	YC2.1	Ratio EYFP/ECFP	Ex 440/Em 480/530	0.8 μM/2 μM	Cytosol and nucleus	Allen et al. (1999); Miyawaki et al. (1999)
	YC3.6	Ratio cpVenus/ECFP	Ex 440/Em 480/530	250 nM	Cytosol and nucleus	Nagai et al. (2004); Mori et al. (2006)
	NES-YC3.6	Ratio cpVenus/ECFP	Ex 440/Em 480/530	250 nM	Cytosol	Krebs et al. (2012)
	NLS-YC3.6	Ratio cpVenus/ECFP	Ex 440/Em 480/530	250 nM	Nucleus	Krebs et al. (2012)
	NUP-YC3.6	Ratio cpVenus/ECFP	Ex 440/Em 480/530	250 nM	Nucleus	Costa et al. (2017)
	4mt-YC3.6	Ratio cpVenus/ECFP	Ex 440/Em 480/530	250 nM	Mitochondria	Loro et al. (2012)
	PM-YC3.6-LTI6b	Ratio cpVenus/ECFP	Ex 440/Em 480/530	250 nM	Plasma membrane	Krebs et al. (2012)
	2Bam4-YC3.6	Ratio cpVenus/ECFP	Ex 440/Em 480/530	250 nM	Chloroplasts and plastids	Loro et al. (2016)
	YC-Nano 65	Ratio cpVenus/ECFP Ratio cpVenus/ECFP	Ex 440/Em 480/530	65 nM	Cytosol and nucleus	Horikawa et al. (2010); Choi et al. (2014)
	SP-YC4.6-ER	Ratio cpVenus/ECFP	Ex 440/Em 480/530	58 nM/14.4 μM	Endoplasmic reticulum	Nagai et al. (2004); Iwano et al. (2009)
	2Bam4-YC4.6	Ratio cpVenus/ECFP	Ex 440/Em 480/530	58 nM/14.4 μM	Chloroplasts and plastids	Loro et al. (2016)
	4mt-D3cpv	Ratio cpVenus/ECFP	Ex 440/Em 480/530	600 nM	Mitochondria	Loro et al. (2013)
	D3cpv-KVK-SKL	Ratio cpVenus/ECFP	Ex 440/Em 480/530	600 nM	Peroxisomes	Palmer et al. (2006); Costa et al. (2010)
	TP-D3cpv	Ratio cpVenus/ECFP	Ex 440/Em 480/530	600 nM	Tonoplast	Krebs et al. (2012)
	CRT-D4ER	Ratio citrine/ECFP	Ex 440/Em 480/530	195 μM	Endoplasmic reticulum	Palmer et al. (2006); Bonza et al. (2013)
Twitch	Twitch 3	Ratio cpCit174/ECFP	Ex 440/Em 480/530	250 nM	Cytosol and nucleus	Thestrup et al. (2014); Waadt et al. (2017)
	Twitch 2B	Ratio cpVenus/mCerulean3	Ex 440/Em 480/530	200 nM	Cytosol and nucleus	Thestrup et al. (2014); Waadt et al. (2017)
CerTN-L15	CerTN-L15	Ratio citrine/cerulean	Ex 440/Em 480/530	1.2 μM	Cytosol and nucleus	Heim et al. (2007); Denninger et al. (2014)
GECOs	R-GECO1	Intensiometric mApple	Ex 561/Em 600	482 nM	Cytosol and nucleus	Zhao et al. (2011); Ngo et al. (2014); Keinath et al. (2015)
	NR-GECO1	Intensiometric mApple	Ex 561/Em 600	482 nM	Nuclear	Zhao et al. (2011); Kelner et al. (2018)
	NR-GECO1.2	Intensiometric mApple	Ex 561/Em 600	1.2 μM	Nuclear	Wu et al. (2013); Kelner et al. (2018); Leitão et al. (2019)
	CG-GECO1	Intensiometric cpGFP	Ex 488/Em 515	749 nM	Cytosol	Zhao et al. (2011); Kelner et al. (2018)
	CG-GECO1.2	Intensiometric cpGFP	Ex 405/Em 515	1.15 μM	Cytosol	Zhao et al. (2011); Kelner et al. (2018); Leitão et al. (2019)
	GEM-GECO1	Intensiometric cpGFP	Ex 405/Em 515	340 nM	Cytosol and nucleus	Zhao et al. (2011); Waadt et al. (2017)
	B-GECO1-mCherry	Ratio cpGFP/mCherry	Ex 405/561/Em 480/600	NA	Cytosol and nucleus	Waadt et al. (2017)
	G-GECO1.1-mCherry	Ratio cpGFP/mCherry	Ex 488/561/Em 515/600	NA	Cytosol and nucleus	Waadt et al. (2017)
	R-GECO1-mTurquoise	Ratio mApple/mTurqouise	Ex 405/561/Em 480/600	NA	Cytosol and nucleus	Waadt et al. (2017)
GCaMPs	GCaMP3	Intensiometric cpGFP	Ex 488/Em 515	542 nM	Cytosol and nucleus	Tian et al. (2009); Nguyen et al. (2018)
	GCaMP5	Intensiometric cpGFP	Ex 488/Em 515	NA	Cytosol and nucleus	Akerboom et al. (2012); Diao et al. (2018)
	GCaMP6f	Intensiometric cpGFP	Ex 488/Em 515	375 nM	Cytosol and nucleus	Chen et al. (2013); Waadt et al. (2017)
	GCaMP6s	Intensiometric cpGFP	Ex 488/Em 515	144 nM	Cytosol and nucleus	Liu et al. (2017); Shao et al. (2020)
	NES-GCaMP6m	Intensiometric cpGFP	Ex 488/Em 515	167 nM	Cytosol	Luo et al. (2020)
	NLS-GCaMP6m	Intensiometric cpGFP	Ex 488/Em 515	167 nM	Nucleus	Luo et al. (2020)
	ER-GCaMP6-210	Intensiometric cpGFP	Ex 488/Em 515	210 μM	Endoplasmic reticulum	de Juan-Sanz et al. (2017); Resentini et al. (2021a)

(continued)

Table 2 Continued

Name	Version	Type	Peaks of excitation/emission (nm)	In vitro K_d for Ca^{2+}[a]	Subcellular localization	References
	GCaMP6f-mcherry	Ratio cpGFP/mCherry	Ex 488/561/Em 480/600	NA	Cytosol and nucleus	Waadt et al. (2017)
	MatryoshCaMP6s	Ratio cpGFP/LSSmOrange	Ex 440/Em 515/600	197 nM	Cytosol and nucleus	Ast et al. (2017)
Case	Case12	Intensiometric cpGFP	Ex 488/Em 515	1 μM	Cytosol and nucleus	Souslova et al. (2007); Zhu et al. (2013)
CEPIA	CRT1a-R-CEPIAer	Intensiometric cpGFP	Ex 561/Em 600	565 μM	Enoplasmic reticulum	Suzuki et al. (2014); Luo et al. (2020)
Aequorin	Aequorin	Bioluminescence	No Ex-/Em 465	7.2–13 μM	Cytosol and nucleus	Knight et al. (1991); Brini et al. (1995)
	Aequorin	Bioluminescence	No Ex-/Em 465	7.2–13 μM	Nucleus	van Der Luit et al. (1999)
	Aequorin	Bioluminescence	No Ex-/Em 465	7.2–13 μM	Chloroplast stroma	Johnson et al. (1995)
	Aequorin	Bioluminescence	No Ex-/Em 465	7.2–13 μM	Mitochondria	Logan and Knight (2003)
	Aequorin	Bioluminescence	No Ex-/Em 465	7.2–13 μM	Golgi	Ordenes et al. (2012)
	Aequorin	Bioluminescence	No Ex-/Em 465	7.2–13 μM	Vacuole/tonoplast	Knight et al. (1996)
YFP-aequorin	CYA	Bioluminescence	No Ex-/Em 465	7.2–13 μM	Cytosol	Mehlmer et al. (2012)
	NYA	Bioluminescence	No Ex-/Em 465	7.2–13 μM	Nucleus	Mehlmer et al. (2012)
	YA	Bioluminescence	No Ex-/Em 465	7.2–13 μM	Plasma membrane	Mehlmer et al. (2012)
	CHYA	Bioluminescence	No Ex-/Em 465	7.2–13 μM	Chloroplast/plastid stroma	Mehlmer et al. (2012); Sello et al. (2016)
	MYA	Bioluminescence	No Ex-/Em 465	7.2–13 μM	Mitochondria	Mehlmer et al. (2012)
	OEYA	Bioluminescence	No Ex-/Em 465	7.2–13 μM	Chloroplast outer envelope	Mehlmer et al. (2012); Sello et al. (2016)
	IEYA	Bioluminescence	No Ex-/Em 465	7.2–13 μM	Chloroplast inner envelope	Mehlmer et al. (2012); Sello et al. (2016)
	TL-YA	Bioluminescence	No Ex-/Em 465	7.2–13 μM	Chloroplast thylakoid lumen	Sello et al. (2018)
	TM-YA	Bioluminescence	No Ex-/Em 465	7.2–13 μM	Chloroplast thylakoid membrane	Sello et al. (2018)
GFP5-aequorin	pchitGFP5:AQ	Bioluminescence	No Ex-/Em 465	NA	Apoplast	Gao et al. (2004)
GFP-aequorin	G5A	Bioluminescence resonance energy transfer	No Ex-/Em 515	NA	Cytosol and nucleus	Baubet et al. (2000); Xiong et al. (2014)

aThe in vitro K_d for Ca^{2+} of the different sensors are those reported in the original works.

reliability brought, in the first years of the 2000s, an "explosion" of different variants, with different Ca^{2+} affinities, different linkers, and different FP pairs (Table 2; Palmer and Tsien, 2006). In 2004, the Miyawaki group developed the Cameleon YC3.60 (often called YC3.6) where the EYFP was replaced with a circularly permuted variant of the Venus FP (cpVenus) (Nagai et al., 2002). The use of the cpVenus as a FRET acceptor greatly increased the energy transfer efficiency from the donor (ECFP), which in practical terms allowed the very reliable performance of in vivo measurements. In fact, in living cells, the simultaneous decrease in ECFP and increase in cpVenus fluorescence emissions, due to FRET, were almost identical to the in vitro analyses (Nagai et al., 2004). This property is of great relevance because it permits ascertaining with high confidence that a change of cpVenus/ECFP ratio, even if small, corresponds to actual FRET levels, thus, a real $[Ca^{2+}]$ change. This latter aspect gains importance when a single cell or single organelle imaging is performed. Moreover, whereas both ECFP and cpVenus might show a pH sensitivity, the FRET ratio is almost unaffected, at least in a narrow change of physiological cytosolic pHs (around pH 7–7.5; Nagai et al., 2004; Behera et al., 2018).

The YC3.6 was expressed in Arabidopsis under the control of the guard cell and pollen-specific promoters, pGC1 and pLat52, respectively, which allowed detecting spontaneous Ca^{2+} oscillations in these two cell types with an improved FRET efficiency (Mori et al., 2006; Yang et al., 2008; Iwano et al., 2009) in comparison to the first YC versions used in plants, the YC2.1 (Allen et al., 1999) and the YC3.1 (Michard et al., 2008; Iwano et al., 2009). The YC3.6 was then expressed under the control of the CaMV35S promoter, making it possible in Arabidopsis to study, at high spatial and temporal resolution, root hair tip Ca^{2+} oscillations (Monshausen et al., 2008). The next step in the exploitation of YC3.6 was obtained by Schumacher's group which placed the sensor with a cytosolic or nuclear localization signal (NES-YC3.6 and NLS-YC3.6) under the control of the pUBQ10 promoter (Grefen et al., 2010; Krebs et al., 2012) that offered a homogeneous expression of the indicator in both Arabidopsis wild-type and mutant backgrounds (Wagner et al., 2015; Teardo et al., 2017; Behera et al., 2018, Corso et al., 2018; Hazak et al., 2019; Wang et al., 2020) as well as in rice (*Oryza sativa*; Behera et al., 2015). YC3.6 was also successfully expressed in the moss *Physcomitrium patens* (formerly *Physcomitrella patens*), allowing the visualization of systemic Ca^{2+} wave propagations in the absence of vascular tissues (Storti et al., 2018). Another important breakthrough was the expression of YC3.6 under the control of the synergid-specific promoter, pMYB98, which allowed the monitoring of Ca^{2+} dynamics in this type of cells during the fertilization process (Hamamura et al., 2014; Ngo et al., 2014). The versatility and reliability of YC3.6 were also demonstrated by its use for the analysis of Ca^{2+} dynamics in different subcellular compartments including mitochondria, chloroplast stroma, and subplasmalemmal space (Table 2; Krebs et al., 2012; Loro et al., 2012, 2016; Storti et al., 2018).

Based on the original work from Nagai et al. (2004) the in vitro K_d of the YC3.6 is 250 nM (Table 2) with a Hill coefficient (Table 3) of 1.7. The knowledge of these two parameters allows the rough conversion of the cpVenus/ECFP ratio into an $[Ca^{2+}]$ if the ratio minimum and ratio maximum are experimentally measured (Palmer and Tsien, 2006; Monshausen et al., 2008; Wagner et al., 2015). One formula that can be used to perform the conversion is the one reported in Monshausen et al. (2008):

$$[Ca^{2+}] = K_d(R-R_{min})/(R_{max}-R_{min})^{1/n},$$

where R represents the cpVenus/ECFP ratio measured at any given time during the experiment, n represents the Hill coefficient, and the K_d the in vitro affinity for Ca^{2+} (Table 3). However, since both the K_d and the Hill coefficients are usually measured in vitro and not in vivo, the ratio conversion into concentration values must be taken with caution. As a matter of fact, a recent work reported for the YC3.6 an in vitro K_d of 719 nM and a Hill coefficient of 2.12 (Li et al., 2021), values that are quite distant from those reported in the original work by Nagai et al. (2004) (250 nM and 1.7, respectively); therefore, pointing out the need for prudence when the conversion is applied (Palmer and Tsien, 2006). Nonetheless, the YC3.6 is indeed a sensor suitable for the analysis of Ca^{2+} dynamics when a given stimulus can induce an increase that is around and above its K_d value. It is also true that in response to stimuli that induce small Ca^{2+} increases, YC3.6 shows some limitations in comparison to the more recent generation of ultrasensitive GECIs (Keinath et al., 2015; Waadt et al., 2017), being in fact not efficient at detecting very subtle changes of $[Ca^{2+}]$ (Keinath et al., 2015). However, the beauty of any genetically encoded sensor is that by following rational and random mutagenesis approaches they can be modified to address specific needs. In 2010, the group of Nagai generated a series of Cameleon variants with higher affinity for Ca^{2+} that were dubbed YC-Nano (Table 2; Horikawa et al., 2010). In particular, the YC-Nano 65 (with an in vitro K_d for Ca^{2+} of 65 nM; Table 2) was efficiently expressed in Arabidopsis and this was instrumental to demonstrate the existence of a long-distance subtle Ca^{2+} wave in seedlings locally challenged with salt stress (Choi et al., 2014). The same sensor was used to compare the cytosolic $[Ca^{2+}]$ at resting and in response to wounding between the wild type and fatty acid oxygenation upregulated 2 (*fou2*) mutant (Lenglet et al., 2017). Very recently, YC-Nano 65 was used to study the response to flg22 in cotyledon and leaf cells in the Arabidopsis wild type, *aca4/aca11* and *aca1/2/7* autoinhibited Ca^{2+}-ATPase mutants (Hilleary et al., 2020; Ishka et al., 2021).

A side-by-side in vivo comparison with plants expressing the YC3.6 and the YC-Nano 65 has not been published yet, but we can predict that the higher affinity for Ca^{2+} of the YC-Nano could saturate in response to different stimuli. Moreover, the different biochemical properties of YC-Nano 65 and YC3.6, like the rate of association (k_{on}) and dissociation (k_{off}) for Ca^{2+} (Table 3), can determine different sensor

Table 3 Brief summary of the principal definitions used to describe GECIs properties

Biochemical parameter	Description
K_d (μM)	Apparent dissociation constant for Ca^{2+} of the sensor, at this concentration, half of the indicators are bound with Ca^{2+}. Given that Hill coefficients are usually higher than 1, the K_d delineates the optimal concentration range at which a GECI should be used.
k_{on} (s^{-1})	Indicates the rate of Ca^{2+} association shown by the sensor, and thus the speed by which a sensor responds to an increase in Ca^{2+} levels.
k_{off} (s^{-1})	Indicates the rate of Ca^{2+} dissociation shown by the sensor, and thus the speed by which a sensor responds to a decrease in Ca^{2+} levels.
Hill coefficient	Indicates the cooperativity of the sensor in the Ca^{2+} binding process. A value greater than 1 indicates that binding of one Ca^{2+} ion facilitates the binding of another. The CaM-based GECI bind four Ca^{2+} ions. The closer to 1 the more linear the output of the reporter.
Dynamic range	For non-ratiometric indicators indicate the maximal fluorescence intensity (typically in a Ca^{2+}-bound state) divided by minimal fluorescence intensity (determined in the presence of EGTA). For ratiometric indicators indicate the maximum fluorescence emissions ratio (typically in a Ca^{2+}-bound state) divided by minimal fluorescence emissions ratio (determined in the presence of EGTA).

dynamics which can be attributed in vivo, as different Ca^{2+} dynamics. We do, therefore, suggest not comparing the published data obtained with these two sensors, but rather, to perform preliminary independent experiments to see which one offers the best readout in relation to the applied stimulus or developmental program under investigation.

An important aspect that needs to be considered is that plants expressing the Cameleon YC3.6 in the cytosol do not show any obvious gross phenotypes, pointing out that the sensor per se does not alter the Ca^{2+} homeostasis and the plant physiology in stable mature plants (Waadt et al., 2017). However, possible effects of Ca^{2+} buffering should be considered in every biological process of interest.

Besides Cameleon and its variants (Table 2), there are other FRET-based sensors that have been successfully used in plants. We can cite here the CerTN-L15 (Heim et al., 2007; Denninger et al., 2014) and the Twitch 2B and 3 (Thestrup et al., 2014; Waadt et al., 2017) that are alternative FRET-based Ca^{2+} sensors which instead of having the CaM domain, use troponin C, a protein exclusively found in myocytes, to sense and bind Ca^{2+}. The substitution of the CaM domain with troponin C prevents any interference due to the endogenous CaM when present at high concentrations such as in the subplasmalemmal region (Miyawaki et al., 1999; Palmer et al., 2006). Plants expressing these two sensors have been shown to properly report [Ca^{2+}] dynamics in synergids and root cells, but their use has so far been limited (Denninger et al., 2014; Waadt et al., 2017). An alternative to the FRET-based sensors might be represented by the use of dimerization-dependent FPs (ddFPs), which is a technology involving the reversible binding of two dark FP monomers to form a fluorescent heterodimeric complex (Alford et al., 2012).

Single FP GECIs

Single fluorophore-based Ca^{2+} indicators GECIs are intensiometric Ca^{2+} sensors, based on a circularly permuted FP (e.g. GFP, YFP, or mApple; Baird et al., 1999; Nakai et al., 2001) fused at its C- and N-termini with the components of a Ca^{2+} sensing module (i.e. CaM domain and the M13 peptide). In the presence of Ca^{2+}, this causes a tightening of the interaction between C- and N-termini of the fluorophore, protecting the chromophore from the environment and leading to increased brightness. In simple words, this interaction induces a dramatic alteration of the spectral properties of the FP with a strong increase in the fluorescence emitted, thus, making these GECIs suitable to indicate Ca^{2+} levels in real time (Nakai et al., 2001). Currently, this principle has been also exploited for the development of different types of biosensors, including kinase activity reporters (e.g. ExRAI; Greenwald et al., 2018).

Similarly to Cameleon, for single FP sensors there was a strong development that yielded a family of GECIs with different colors, different Ca^{2+} affinities, different Hill coefficients, less pH sensitivity, and with improved signal-to-noise ratio (Table 2; Zhao et al., 2011). Just to cite an example, from 2001 to 2019, there has been an evolution that has led from the GCaMP to the jGCaMP7 (Figure 1; Nakai et al., 2001; Tian et al., 2009; Akerboom et al., 2012; Chen et al., 2013; Greenwald et al., 2018; Dana et al., 2019). The aim to improve GCaMPs was driven by the necessity to increase the sensitivity and kinetics of the sensors, trying to make them closer, in terms of properties, to the synthetic Ca^{2+} dyes that for the needs of neuroscience are still among the most sensitive and rapid Ca^{2+} indicators. It is worth considering that in plant cells, the kinetics of the sensor response does not represent a big limitation, since in most of the published works the imaging sampling was set at every 2–5 s (e.g. guard cells, pollen tubes and root hair growth, and root tip cells; Allen et al., 1999; Monshausen et al., 2008; Yang et al., 2008; Michard et al., 2011; Candeo et al., 2017; Li et al., 2021; Resentini et al., 2021a). Instead, the ease of use and the sensitivity of single FP GECIs are good properties that have pushed the plant community to move toward their use. The fact that single FP GECIs rely on a single excitation and a single emission makes them particularly suitable to be combined with other fluorescent markers or sensors, and for their use with simple and accessible microscope equipment (Table 1). The first single FP GECI expressed in plant cells were the GFP-based Ca^{2+} indicator Case12 (Zhu et al., 2013) and the red-shifted R-GECO1 (Ngo et al., 2014; Keinath et al., 2015). The latter is a red

fluorescent GECI derived from the GCaMP3 (Tian et al., 2009), where the circularly permuted GFP (cpGFP) was substituted with the cpmApple (Zhao et al., 2011). Importantly, R-GECO1 is excited with green light (e.g. 561 nm; Table 2) which besides offering a greater tissue penetration neither stimulates photosynthesis nor photoreceptors (Taiz et al., 2014), making it particularly suited for use in green tissues. In 2015, R-GECO1 was first used in a series of "classical experiments" in Arabidopsis root meristems, treated with external ATP and pathogen elicitors such as flg22 and chitin, and demonstrating the very high sensitivity of this sensor (Keinath et al., 2015). It must be said that the same sensor was also previously expressed in pollen tubes used to fertilize an Arabidopsis line expressing the Cameleon YC3.6 in synergids, thus enabling Ca^{2+} imaging in two different tissues (Ngo et al., 2014). The in vitro K_d of R-GECO1 of 482 nM (Table 2) with a Hill coefficient of 2.06 (Zhao et al., 2011) makes this sensor suitable to efficiently detect cytosolic Ca^{2+} variations, and its constitutive expression under the pUBQ10 promoter in the stable Arabidopsis line does not produce gross and visible phenotypes (Waadt et al., 2017; Resentini et al., 2021a). Instead, when other color variants of the GCaMP3 (e.g. GEM-GECO1, B-GECO1, and G-GECO1.1; Table 2) were stably expressed in Arabidopsis, the plants showed some growth defects (Waadt et al., 2017). This negative effect on plant physiology indicates that these reporters with a higher Hill coefficient for GEM- (2.94) and B-GECO1 (2.64) or a lower Ca^{2+} affinity for the G-GECO1.1 (K_d 618 nM; Zhao et al., 2011) might potentially act as Ca^{2+} buffers, but this needs to be demonstrated. Overall, as a good practice, it is advised to compare the phenotype of a chosen sensor line with wild-type plants in the context of a given process of interest, and never to forget that the sensor could have a potential effect on plant physiology.

The GCaMP3 is a relatively old GCaMP version (Tian et al., 2009), and neuroscientists have now moved to the use of the most recent versions (GCaMP6 and jGCaMP7). Nevertheless, GCaMP3 was only recently expressed in *Nicotiana benthamiana*, Arabidopsis, and *P. patens* (Figure 1; DeFalco et al., 2017; Kleist et al., 2017; Vincent et al., 2017; Nguyen et al., 2018; Toyota et al., 2018; Krogman et al., 2020) and allowed the detection of bright long-distance leaf-to-leaf Ca^{2+} waves (Toyota et al., 2018; Nguyen et al., 2018). GCaMP3 has been also expressed under the control of tissue-specific promoters (i.e. phloem and different root tissues; Vincent et al., 2017; Toyota et al., 2018; Krogman et al., 2020).

Similarly to EYFP/ECFP FRET-based sensors, GCaMPs come with some disadvantages, as the blue excitation light can stimulate photosynthesis (Taiz et al., 2014) and can trigger in itself $[Ca^{2+}]_{cyt}$ increase via phototropins (Zhao et al., 2013; Ishka et al., 2021). This could be avoided using R-GECO1, which being excited with green light is possibly more compatible with long-term imaging in the shoot. Other GCaMP versions, such as GCaMP5, GCaMP6f, and GCaMP6s (Table 2; Zhu et al., 2013; Liu et al., 2017; Vincent et al., 2017; Diao et al., 2018; Shao et al., 2020; Suda et al., 2020; Ishka et al., 2021) as well as other green and red variants of GECO1 (CG-GECO1.2 and R-GECO1.2; Kelner et al., 2018; Table 2) have also been used in plant cells.

Such a wealth of available tools might, however, generate some confusion in choosing one version over another. Indeed, the different GCaMP variants have different colors, different K_d for Ca^{2+} which make them suitable for use in different compartments or, similarly to the use of the YC-Nano 65, to report subtle changes of $[Ca^{2+}]$. As an example, when subtle changes of $[Ca^{2+}]$ are expected, the high affinity for Ca^{2+} of GCaMP6s (K_d of 144 nM) is more suitable than GCaMP3 (K_d of 542 nM) or GCaMP6f (K_d of 375 nM; Table 2). However, a complete side by side comparison of all different sensors used in plant cells is not available, with only some tested by Waadt et al. (2017). Possibly an interested researcher should preliminarily test them to identify the best one for each experimental condition. We are currently working with both R-GECO1 and GCaMP3 expressing plants, and overall, they provide similar results. Nevertheless, as anticipated above, the most recent generation of single FP GECIs is continuously improving to increase the sensitivity and the signal-to-noise ratio to perform imaging in neuronal tissues, which might also be useful for plant scientists. As a matter of fact, all the single FP GECIs exploit an OFF/ON response with a negligible fluorescent signal in the Ca^{2+} unbound state and strong fluorescence with even relatively small changes in $[Ca^{2+}]$. Such a property represents a big advantage when imaging an entire plant. Indeed, both GCaMP3 and R-GECO1 have demonstrated that they offer enough sensitivity to detect and measure Ca^{2+} wave propagation between leaves in adult Arabidopsis plants in response to wounding or insect chewing (Nguyen et al., 2018; Toyota et al., 2018; Resentini et al., 2021a; Table 1). This result represents a major achievement in the field that was brought to a new dimension when the GCaMP6f was expressed in the carnivorous plant *Dionaea muscipula*, also known as Venus flytrap (Figure 1; Suda et al., 2020). The Venus flytrap rapidly closes the valves following mechanical stimulation of "sensitive hairs" and a role of Ca^{2+} as a second messenger in the closing mechanism was previously hypothesized (Scherzer et al., 2015; Hedrich and Neher, 2018). By using the GCaMP6f, Suda et al. (2020) demonstrated that the stimulation of the sensory hairs had the effect of inducing a Ca^{2+} wave that propagated throughout the entire leaf blade at a speed greater than 20 mm/s (Suda et al., 2020). Such a propagation rate exceeds at least 20 times the Ca^{2+} response to leaf injury in Arabidopsis (Toyota et al., 2018; Shao et al., 2020), and thus requires GECI with fast k_{on}-kinetics such as the GCaMP6f.

In conclusion, the use of different single FP GECIs provides reliable data and offers the chance to capture dynamic processes in multicellular adult organisms, opening opportunities to explore new hypotheses. Also, Cameleon sensors allow the performance of large imaging experiments (Beneloujaephajri et al., 2013; Benikhlef et al., 2013; Costa et

al., 2017; Behera et al., 2018; Doccula et al., 2018; Hilleary et al., 2020; Ishka et al., 2021), but for their use, a piece of more sophisticated and expensive equipment is required, whereas single FP GECIs need a simple single excitation, single emission fluorescence microscope equipped with a good camera (Table 1; Vincent et al., 2017; Nguyen et al., 2018; Toyota et al., 2018; Resentini et al., 2021a).

A notable disadvantage of the single FP GECI is that the obtained intensities are not only determined by Ca^{2+} levels but are also dependent on local expression levels and can be quenched at low pH.

Organellar calcium dynamics: state of the art

The contribution of organellar Ca^{2+} handling in the regulation of signaling processes has been recently reviewed, so we will redirect interested readers to those papers (Stael et al., 2012; Costa et al., 2018; Pirayesh et al., 2021; Resentini et al., 2021b). Nevertheless, here, we briefly summarize what GECIs are available for the study of Ca^{2+} dynamics in subcellular compartments and which tools, among those recently developed, we foresee for the advancement of the field. Table 2 is an updated version of the table published in Costa et al. (2018) and reports the most available Arabidopsis lines expressing subcellular targeted GECIs.

Aequorin was targeted to the cytosol, nucleus, mitochondria, Golgi apparatus, tonoplast, apoplast, chloroplast, and chloroplasts' subcompartments (Knight et al., 1991, 1996; Johnson et al., 1995; van Der Luit et al., 1999; Logan and Knight, 2003; Gao et al., 2004; Mehlmer et al., 2012; Ordenes et al., 2012; Sello et al., 2016, 2018). One needs to bear in mind that aequorin can offer only an averaged response of organelles or subcellular compartments from different cells and often from multiple plants. Therefore, in the case of the requirement of single organelles, the use of fluorescent GECIs is required.

Both FRET-based cameleon and single FP sensors were targeted to different subcellular locales, allowing the detection of Ca^{2+} dynamics within different compartments with, in some cases, a single cell or even single organelle resolution (Iwano et al., 2009; Costa et al., 2010, 2013; Krebs et al., 2012; Loro et al., 2012, 2016; Bonza et al., 2013; Kelner et al., 2018; Leitão et al., 2019; Resentini et al., 2021a). A special mention is needed for the simultaneous expression, in *Medicago truncatula* and Arabidopsis, of the G-GECO1.1 (and 1.2) and R-GECO1.1 (and 1.2) sensors targeted, respectively, to the cytosol and nucleus (Kelner et al., 2018; Leitão et al., 2019). High-resolution imaging of these sensors in Medicago root hairs revealed that in response to Nod-Factors, the nuclear Ca^{2+} increase preceded the cytosolic one (Kelner et al., 2018). Similarly, a nuclear spontaneous Ca^{2+} increase anticipated the cytosolic one in Arabidopsis root tip meristematic cells during growth (Leitão et al., 2019). Moreover, the use of Cameleon YC3.6 targeted to mitochondria and nucleus enabled the simultaneous imaging of Ca^{2+} in these two compartments in Arabidopsis guard cells challenged with osmotic stress (Loro et al., 2012) or root tip cells in response to ATP (Loro et al., 2013).

At the present time, most of the Ca^{2+} analyses in subcellular compartments have been carried out with Cameleon variants, and only limited use of recent generation GECIs has been exploited (reviewed in Costa et al., 2018; Luo et al., 2020). The trend is different in animal cells, where more recent GECIs have been used in different subcellular compartments. Modified GCaMP6, CEPIA, and RCaMP sensors (Greenwald et al., 2018) with different spectral features or lower affinities for Ca^{2+} have shown to be suitable for analyses of Ca^{2+} dynamics in the endoplasmic reticulum (ER) and mitochondria of single neurons in response to APs (Suzuki et al., 2014; Dana et al., 2016; de Juan-Sanz et al., 2017; Ashrafi et al., 2020). Hence, this is the right time to explore the use of these sensors in plants, as they can offer some advantages compared with Cameleon sensors, although there are other limitations. The use of Cameleon sensors for the analysis of Ca^{2+} dynamics in subcellular compartments is primarily justified by its ratiometric nature that helps to reduce artifacts when measuring Ca^{2+} in moving organelles at high magnification or when comparing the steady-state concentration (Table 1; Wagner et al., 2015; Corso et al., 2018). As an example, based on our own experience, the large size of Cameleon (~73 KDa) may pose some limitations for its proper targeting. In the case of mitochondria, ER, and chloroplasts, the Cameleon targeting required tailored strategies. To prevent a cytosolic mislocalization of the Cameleon (i) the mitochondrial targeting sequence had to be repeated four times (Palmer et al., 2006; Loro et al., 2012), (ii) the targeting to the ER required both a KDEL sequence at the C-terminus end plus a plant-specific calreticulin targeting sequence at the N-terminus end of the sensor (Palmer et al., 2004; Iwano et al., 2009; Bonza et al., 2013), and (iii) the targeting to the chloroplast stroma needed to double the BETA-AMYLASE 4 (Bam4) targeting sequence (Loro et al., 2016). The proper targeting of the Cameleon was indeed obtained, but this was at the expense of different issues, such as a more difficult design of the construct, and silencing. As an example, a strong silencing was relevant when the Cameleon was targeted to chloroplasts (2Bam4-YC3.6). In fact, the generation of stable fluorescent plants could be obtained only in the Arabidopsis *RNA-dependent RNA polymerase-6-11* (*rdr6-11*) mutant background which is compromised in silencing (Peragine et al., 2004; Loro et al., 2016). Nevertheless, with the ER-targeted version of the Cameleon (CRT-D4ER), its expression was also limited to juvenile tissues, with some difficulties found in expressing it in some T-DNA lines (Corso et al., 2018; Shkolnik et al., 2018). We hope that the use of single FP GECIs might reduce silencing issues. A recent publication has reported the use of the ER-localized CRT1a-R-CEPIAer sensor and no issues related to silencing were highlighted (Luo et al., 2020). We have also successfully expressed the ER-GCaMP6-210 sensor localized in the ER (Table 2; de Juan-Sanz et al., 2017; Resentini et al., 2021a) in Arabidopsis wild-type and R-GECO1 backgrounds, offering the possibility to perform the

simultaneous Ca^{2+} imaging in the ER and cytoplasm of adult plants (Resentini et al., 2021a). This result was not reached with the CRT-D4ER, not even in the ER alone, where the fluorescence was lost with aging.

We foresee that in the coming years, the use of single FP GECIs for the analyses of organellar Ca^{2+} dynamics should accompany the use of Cameleon, in particular for the simultaneous analysis of Ca^{2+} dynamics in different compartments, by combining sensors with different excitation and emission spectra (Resentini et al., 2021a). Moreover, organellar-targeted single FP GECIs should also be employed to analyze Ca^{2+} dynamics in adult plants, by exploiting their high sensitivity and dynamic range (Table 3).

Ratiometric versus intensiometric GECIs: a practical guide for their choice

In this Update article, we have referred several times to the advantages offered by using ratiometric FRET-based sensors compared with intensiometric ones. In this section, we want to further discuss this statement. Traditionally, ratiometry-based Ca^{2+} recordings rely completely on ratio changes, and these measurements are not influenced by the actual amount of the indicator or by changes in the focusing position of the imaging system (Rudolf et al., 2003). This is particularly true with FRET-based sensors since the fluorescence emission from the acceptor depends on the light absorbed by the donor, and a single excitation is used, requiring a single excitation light path. In practical terms, one of the advantages of using a FRET-based ratiometric sensor, like Cameleon, is that there is the possibility to efficiently compare the steady-state ratios among different genotypes or in the same genetic background in response to long-term treatments. This is true for different subcellular compartments such as cytosol, mitochondria, and ER (Laanemets et al., 2013; Wagner et al., 2015; Lenglet et al., 2017; Yang et al., 2017; Behera et al., 2018; Corso et al., 2018; Doccula et al., 2018; Shkolnik et al., 2018; Fasani et al., 2019; Hilleary et al., 2020; Ishka et al., 2021). Another advantage of ratiometric FRET-based sensors is that the results can be presented as raw acceptor/donor fluorescence emissions ratios (e.g. cpVenus/ECFP) without the need for calibration. Our direct experience with intensiometric sensors has revealed that the fluorescence is already variable at resting conditions, even within the same genetic background grown in the same conditions (Figure 3, B). To obviate the fluorescence variability among samples, when R-GECO1 or GCaMPs are used, the data are often presented as normalized fluorescence and not as absolute values (Vincent et al., 2017; Dindas et al., 2018; Nguyen et al., 2018; Toyota et al., 2018; Resentini et al., 2021a). Usually, this does not represent a problem; however, the need to rely on normalization may represent an issue for a correct interpretation of the results. To support this statement, we here present a set of experimental data that help to better clarify this point.

Arabidopsis seedlings expressing the Cameleon YC-Nano 65 and the R-GECO1 were germinated and grown in a standard growth half-strength MS medium and at 6-d-old stage were independently incubated for 10 min in solutions with different concentrations of Ca^{2+} (0-calcium and 1.5 mM calcium) and imaged with the wide field microscope setup described in Behera et al. (2018) (Supplemental Materials and Methods). After 10-min incubation, the root tip cells of the seedlings were imaged while keeping them in continuous perfusion before a 3-min pulse treatment with 10 μM of the synthetic auxin 1-naphthylacetic acid (NAA). For each experiment, the cpVenus/ECFP ratio for YC-Nano 65 and single fluorescence changes for R-GECO1 were measured over 20 min. The data were plotted over time as both normalized ($\Delta R/R_0$ and $\Delta F/F_0$) or raw cpVenus/ECFP ratios and R-GECO1 fluorescence (Figure 3, C, D, G, and H). At the end of the experiment, four sets of data could be compared: (i) YC-Nano 65 seedlings treated with 10 μM NAA in 0-calcium; (ii) YC-Nano 65 seedlings treated with 10 μM NAA in 1.5 mM calcium; (iii) R-GECO1 seedlings treated with 10 μM NAA in 0-calcium, and (iv) R-GECO1 seedlings treated with 10 μM NAA in 1.5 mM calcium. The results showed that NAA induced an increase in the cpVenus/ECFP ratio and R-GECO1 fluorescence that corresponds to a $[Ca^{2+}]_{cyt}$ increase (Figure 3, C and D), as previously demonstrated (Behera et al., 2018). Interestingly, by comparing the maximum change of normalized cpVenus/ECFP ratio and R-GECO1 fluorescence, it was clear that the $[Ca^{2+}]_{cyt}$ increase was higher in the medium with 1.5 mM calcium than the one observed with 0-calcium (Figure 3, E and F). Thus, both sensors reported the same result, suggesting that the amplitude of the NAA-induced cytosolic Ca^{2+} increase depends on the availability of Ca^{2+} in the medium. However, comparison of the raw cpVenus/ECFP ratio and non-normalized R-GECO1 fluorescence changes provided a different result (Figure 3, G and H). In fact, the incubation of seedlings in 0-calcium had the opposite effects in the two sensor lines. On the one hand, the YC-Nano 65 showed a higher ratio at resting (Figure 3, A and G) with a relatively smaller differential response to NAA treatment as evidenced by the normalized data (Figure 3, E), despite the raw maximum signal being higher than in 1.5 mM calcium (Figure 3, I). On the other hand, the resting R-GECO1 fluorescence (Figure 3, B) was lower in 0-calcium compared with 1.5 mM calcium with corresponding reductions in NAA response (Figure 3, F and J). In conclusion, both sensors reported a decreased NAA response, when Ca^{2+} was removed from the media, but with different starting points, de facto with opposite results.

Since it has been reported that R-GECO1 may suffer from a pH sensitivity (Zhao et al., 2011; Keinath et al., 2015), we measured the cytosolic pH in root tip cells of Arabidopsis seedlings using the ratiometric pH sensor pH-GFP (Moseyko and Feldman, 2001; Behera et al., 2018) in response to 0-calcium treatment (Figure 4). The experiment clearly showed that shifting from 1.5 mM calcium to 0-calcium led to a cytosolic acidification (Figure 4, A and B). Thus, the incubation with 0-calcium can have multiple effects, including changing the cytosolic pH. Such acidification may quench the R-

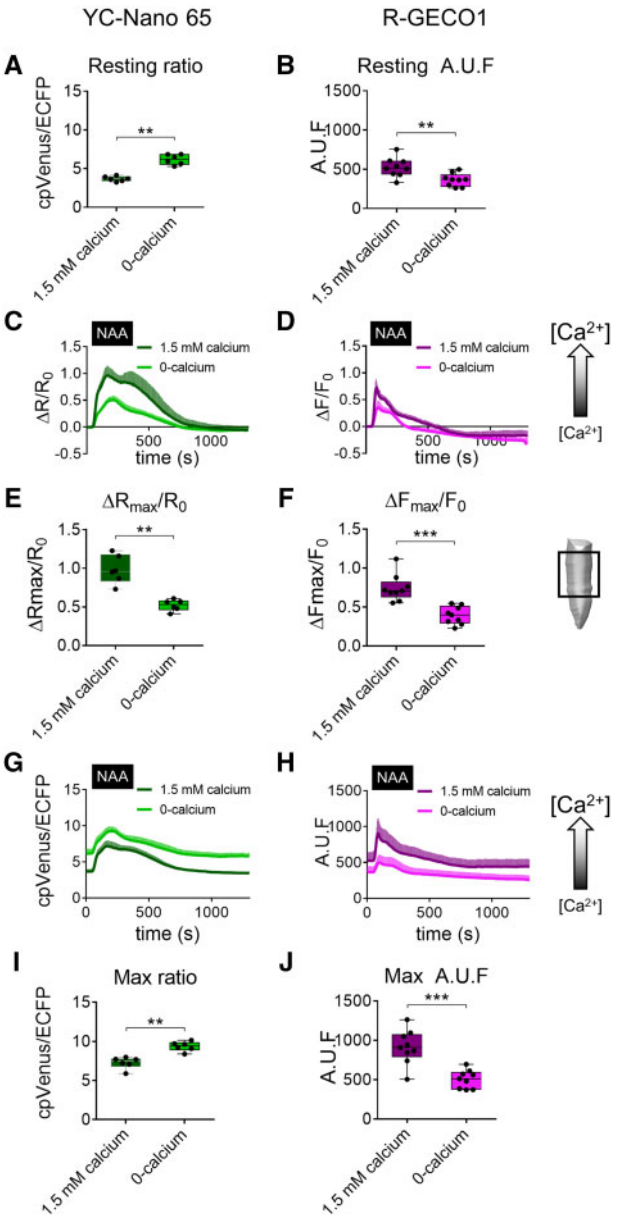

Figure 3 Comparison of the Ca^{2+} response in root tip cells expressing YC-Nano 65 or R-GECO1. Seedlings were exposed to a pulse of 10 μM NAA and medium containing either 1.5 mM calcium ($CaCl_2$) or 0-calcium. The schematic drawing on the right shows the root tip region examined. A, cpVenus/ECFP ratio at rest in root tip cells of YC-Nano 65 seedling in 1.5 mM calcium and 0-calcium. B, R-GECO1 fluorescence at rest in root tip cells of R-GECO1 seedlings in 1.5 mM calcium and 0-calcium. C, Normalized averaged YC-Nano 65 cpVenus/ECFP ratios (R) ($\Delta R/R_0 = (R-R_0)/R_0$) over time in root tip cells in response to NAA as indicated by the black box on the x-axis. D, Normalized averaged R-GECO1 fluorescence (F) ($\Delta F/F_0 = (F-F_0)/F_0$) over time in root tip cells in response to NAA as indicated by the black box on the x-axis. R_0 and F_0 are the prestimulus values of R and F, respectively. The shaded right-side arrow indicates the direction of the $[Ca^{2+}]_{cyt}$ increase. E, Maximal relative amplitude as $\Delta R_{max}/R_0$ of cpVenus/ECFP ratio triggered by NAA in 1.5 mM calcium and 0-mM calcium conditions. F, Maximal relative amplitude as $\Delta F_{max}/F_0$ of R-GECO1 fluorescence triggered by NAA in 1.5 mM calcium and 0-calcium conditions. G and H, Same experiments shown in (C and D) without normalization to the pre-stimulus situation. The shaded right-side arrow indicates the direction of the $[Ca^{2+}]_{cyt}$ increase. I, Maximal amplitude of cpVenus/ECFP ratio triggered by NAA application in 1.5 mM calcium and 0-calcium. J, Maximal amplitude of R-GECO1 fluorescence triggered by NAA application in 1.5 mM calcium and 0-calcium. Arbitrary units of fluorescence (AUF). $n \geq 6$. Data were plotted as box-and-whisker plots using GraphPad, in which all the experimental points are plotted, and their distribution represented as a box that extends from the 25th to 75th percentiles. The line in the middle of the box is plotted at the median. P values were calculated with an unpaired Student's t test. Error bars = SD. $^{**}P \leq 0.005$, $^{***}P \leq 0.0005$ (t test).

GECO1 fluorescence, reducing its dynamic range. On the other hand, even considering that the pH can also affect the cpVenus and ECFP fluorescence of the YC-Nano 65 Cameleon (Supplemental Figure S1) the ratio calculation seems to better correct for this potential issue as previously shown for the YC3.6 (Nagai et al., 2004; Behera et al., 2018).

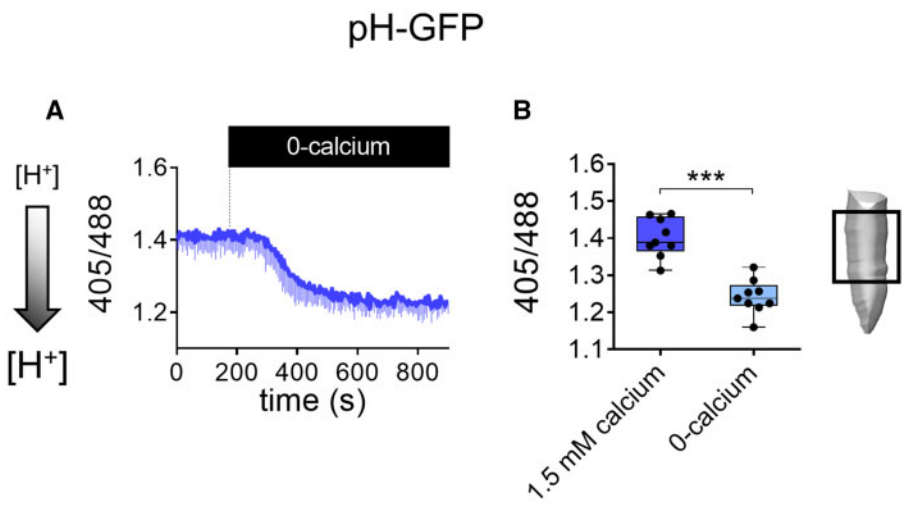

Figure 4 Cytosolic pH dynamics in root tip cells in response to 0-calcium treatment. A, pH dynamics in pH-GFP root tip cells of the region indicated in the schematic drawing, treated with medium with 0-calcium (from 1.5 mM calcium to 0-calcium) as indicated by the black box on the *x*-axis. The ratio corresponds to the emission of the pH-GFP sensor when excited with light at 405 nm divided by the emission of the sensor when excited at 488 nm. B, The amplitude of 405/488 ratio in 1.5 mM calcium and 0-calcium. $n = \geq 5$. The shaded left-side arrow indicates the direction of the pH decrease. Data were plotted as box-and-whisker plots using GraphPad, in which all the experimental points are plotted, and their distribution represented as a box that extends from the 25th to 75th percentiles. The line in the middle of the box is plotted at the median. *P* values were calculated with an unpaired Student's *t* test. Error bars = SD. $^{***}P \leq 0.0005$ (*t* test).

The understanding of how 0-calcium treatment affects both cytosolic Ca^{2+} and pH is currently under investigation. Nevertheless, our example illustrates that different treatments can potentially alter the properties of the sensors and warranting a careful comparison among them.

This series of experiments demonstrate that intensiometric sensors can be prone to artifacts and that whereas they show superior sensitivity compared with FRET sensors (Krebs et al., 2012; Keinath et al., 2015; Waadt et al., 2017; Resentini et al., 2021a), they might lead to a wrong interpretation of the results. This fact does not signify that intensiometric sensors are not reliable, but that depending on the type of experiment being done, some additional controls should be carried out. In light of this, the use of the recently developed transcriptionally linked dual sensors, such as the CapHensor which allows the simultaneous analysis of Ca^{2+} and pH dynamics (Li et al., 2021) or the R-GECO1-GSL-E^2GFP to simultaneously monitor Ca^{2+}, H^+, and Cl^- (Waadt et al., 2020) could be an option. Of particular note, the development of different dual sensor reporters to simultaneously monitor the dynamics of Ca^{2+} with other ions, analytes, or redox potentials of different redox couples will represent an important tool to reach an integrated picture of the physiological response to different stimuli (Wagner et al., 2019; Waadt et al., 2020).

Despite the reservations made on the pH sensitivity of single FP GECIs, to correct for variation in expression levels, in frame, or nested fusions of single FP GECI with other FPs have been developed (Ast et al., 2017; Waadt et al., 2017, 2020). Specifically, Waadt et al. (2017) generated a construct where the mTurquoise FP (Goedhart et al., 2010) was introduced in a vector harboring the R-GECO1 (Table 2). Since mTurquoise fluorescence emission is independent of a change in $[Ca^{2+}]$, this strategy allowed the authors to use it as a reference (Waadt et al., 2017). The ratiometric R-GECO1-mTurquoise allowed the authors to reveal detailed maps of $[Ca^{2+}]$ changes in response to auxin and ATP in root tip cells (Waadt et al., 2017). A different approach aimed at generating a ratiometric GCaMP sensor was followed by the Frommer's group, which adopted a strategy based on the employment of a single FP-cassette that nests a stable reference FP (large Stokes shift LSSmOrange) within the GCaMP6s reporter that was brought to the generation of the MatryoshCaMP6s sensor (Table 2; Ast et al., 2017). The main difference between the two approaches is that the "MatryoshCaMP6s sensor" requires a single excitation with a dual emission, instead of the two excitations and two emissions required for the R-GECO1 and mTurquoise, respectively. Indeed, similarly to Cameleon, the use of a second FP may limit the use of the Ca^{2+} sensor with other markers or biosensors. The availability of the R-GECO1-mTurquoise ratiometric sensor or a similar design for a GCaMPs-mCherry (Waadt et al., 2017) can represent a good compromise for the correction of artifacts, potentially also reducing the pH sensitivity. However, the need for dual excitation and dual emission may still limit their use: whereas the MatryoshCaMP6s has again an increased size that could introduce other limitations. Alternatively, dual excitation single FP GECIs could be used, such as GEX-GECO and REX-GECO (Zhao et al., 2011; Wu et al., 2014). Unfortunately, the latter are relatively dim and need further optimization. Interestingly, a kinase activity sensor based on GCaMP3 displayed two excitation peaks with a similar sensitivity to pH changes between 5.6 and 10 (Mehta et al., 2018), suggesting that the ratiometric excitation imaging of this kinase sensor is relatively insensitive to pH changes. Therefore, it seems

possible to engineer an excitation ratiometric GECI for normalization to expression levels and pH changes, based on the bright single FP GCaMP3. A reasonably up-to-date database of currently available genetically encoded sensors can be found at BiosensorDB.ucsd.edu.

Microscopy techniques for plant calcium imaging

Traditionally, Ca^{2+} imaging has been carried out by using standard wide field and confocal fluorescence microscopy, while imaging of aequorin has been usually performed with back-illuminated charge-coupled device (CCD) cameras equipped with a light-tight box. The first Ca^{2+} analyses performed in single cells, like stomatal guard cells, root hairs, and pollen tubes, were carried out with microscopes using high magnification objectives. However, when Ca^{2+}-sensitive dyes were the only available sensors it was difficult to image more than one cell per experiment (e.g. McAinsh et al., 1995; Ehrhardt et al., 1996; Holdaway-Clarke et al., 1997; Garcia-Mata et al., 2003). Instead, using transgenic plants, stably expressing GECIs, it was possible to measure Ca^{2+} dynamics both at single cell level (Allen et al., 1999; Monshausen et al., 2008; Loro et al., 2012; Hilleary et al., 2020) and in the entire organs or tissues, by decreasing the magnification (Kiegle et al., 2000; Krebs et al., 2012; Zhu et al., 2013; Kiep et al., 2015; Yuan et al., 2014; Jiang et al., 2019; Chen et al., 2020; Hilleary et al., 2020; Wu et al., 2020; Ishka et al., 2021).

To perform Cameleon-based Ca^{2+} imaging, a wide field microscope with one filter for the excitation and one for the emission are not sufficient, whereas this configuration is suitable for a single FP GECI. The use of Cameleon requires the detection of the emissions from two FPs obtained by performing a quick change of filters with a filter wheel that therefore needs repetition of the excitation step. An alternative configuration exploits a beam splitter coupled to one or two cameras to simultaneously acquire the two fluorescence signals (e.g. cpVenus and ECFP). The use of a beam splitter configuration for Cameleon detection was recently reported with a stereomicroscope, allowing the performance of a FRET-based analysis in entire Arabidopsis cotyledons and young leaves expressing the YC-Nano 65 (Hilleary et al., 2020; Ishka et al., 2021). With the wide field microscope, single cell resolution can be obtained when imaging guard cells from an epidermal strip preparation or in vitro germinated pollen tubes, but the lack of optical sectioning hinders the analysis of Ca^{2+} dynamics at single cell level in an entire organ (Table 4). Nevertheless, the use of tissue-specific promoters to guide the expression of the sensor in a given cell type allows the performing of single cell analysis in intact leaves by means of wide field microscopy (Yang et al., 2008). However, in cases where the sensor is ubiquitously expressed, to obtain single cell resolution an optical sectioning microscope is needed. The most widely used optical sectioning technique is the confocal microscope, which makes use of a pinhole to reject the light coming from sample positions that are not in focus. In this configuration, a single laser (445 or 458 nm to excite the acceptor) and two photomultipliers are sufficient for FRET imaging, allowing many plant-biology laboratories to perform Ca^{2+} imaging experiments at high spatial resolution (Tanaka et al., 2010; Loro et al., 2012; Costa et al., 2013; Krebs and Schumacher, 2013; Choi et al., 2014). When required to perform Ca^{2+} imaging analysis at a high temporal resolution, the laser scanning confocal microscope shows some limitations in terms of acquisition speed (Table 4). The sampling is in the order of 1 s, with a traditional galvo scanner. As an example, with a pixel number of 1024 × 1024, a typical acquisition frequency is 0.5 Hz, whereas with a half resolution of 512 × 512 it is 1 Hz. For a higher sampling rate, a spinning disk confocal is a possible choice, as it essentially parallelizes the confocal pinhole detection (Table 4). However, in this case, the need for simultaneous acquisition of both fluorescent ECFP and cpVenus emissions as well as the need for a dedicated laser (i.e. 445 nm) increases the complexity and the price of the microscope setup (Table 4). To gain access to a high resolution, high speed FRET acquisition, we developed a tailored fluorescent light sheet fluorescence microscope that allowed us to perform single cell imaging with a fast rate of acquisition as well as long-term developmental analyses (Costa et al., 2013; Candeo et al., 2017; Romano Armada et al., 2019; Alfieri et al., 2020; Table 4). To do experiments with plants expressing single FP GECIs, the same microscopes described above can be used with standard configurations for a single excitation and a single emission, de facto expanding the audience of possible users. The more recent generation of single FP GECIs has largely facilitated Ca^{2+} imaging analyses since relatively low-cost cameras with good sensitivity exist, which can provide reliable measurements. This is shown in recent papers demonstrating that stereomicroscopes equipped with standard CCD or complementary metal–oxide–semiconductor (CMOS) cameras and common light sources like fluorescent lamps or LED illumination systems are suitable to perform analyses of Ca^{2+} dynamics in entire adult plants (Vincent et al., 2017; Nguyen et al., 2018; Toyota et al., 2018; Shao et al., 2020; Suda et al., 2020; Resentini et al., 2021a) whereas, traditionally, the Ca^{2+} analyses were mainly confined to root cells of Arabidopsis, rice seedlings or a limited number of leaf epidermal cells (Krebs et al., 2012; Loro et al., 2012; Behera et al., 2015; Keinath et al., 2015; Waadt et al., 2017; Table 4).

Future developments

Here, we take the opportunity to foresee possible future developments. Whereas single FP GECIs may be prone to artifacts we still foresee an extensive use of them by harnessing their unique properties. As an example, having GECIs emitting at different wavelengths allows one to study Ca^{2+} dynamics in different subcellular compartments, within the same cell. This has been largely carried out in animal cells, but the applications in plants are still limited (Greenwald et al., 2018; Kelner et al., 2018; Resentini, 2021a). We anticipate

Table 4 Summary of advantages and limitations of different microscopy systems suitable for Ca^{2+} imaging

Type of microscopy	Advantages	Limitations
Wide field microscopy	(i) Suitable for its use with FRET-based and single FP GECI; (ii) single cell resolution allowed with specific sample preparations (e.g. Guard cells in epidermal strips).	(i) Lack of optical sectioning.
Laser scanning confocal microscopy	(i) Optical sectioning allowed; (ii) spectral separation with multiple detectors; (iii) single cell analyses allowed in entire organs; (iv) most of the commercial configurations allow FRET analyses.	(i) Acquisition speed.
Spinning disk confocal microscopy	(i) Fast rate of acquisition; (ii) optical sectioning allowed; (iii) single cell analyses allowed in entire organs; (iv) lower phototoxicity.	(i) High price.
Light sheet fluorescence microscopy	(i) Fast rate of acquisition; (ii) optical sectioning allowed; (iii) single cell analyses allowed in entire organs; (iv) long-term analyses; (v) tailored design.	(i) Low versatility.

that we could express GCaMP sensors, in mitochondria or in the ER together with the R-GECO1 localized to the cytosol or other combinations. By producing plasmids that harbor both sensors in the same backbone (Waadt et al., 2020; Li et al., 2021) we can transform different (single or multiple) mutants to identify and study the Ca^{2+} transport mechanisms in the different membranes (e.g. Wagner et al., 2015; Corso et al., 2018; Kelner et al., 2018). R-GECO1 or other red shifted variants (e.g. K-GECO1 or R-CaMPs; Shen et al., 2018) can be expressed together with Cameleon or other FRET-based GECIs. To perform simultaneous Ca^{2+} imaging analyses in different tissues, different GECIs can be expressed in the same plant under the control of different tissue-specific promoters (Ngo et al., 2014).

At the same time, optical imaging techniques could play a relevant role in the study of Ca^{2+} dynamics at different spatial scales. Super-resolution microscopy, the field of optical imaging that goes beyond the diffraction limit, is having an increased rate of application in plant biology (Komis et al., 2015; Shaw et al., 2019) even if its use in Ca^{2+} studies is still limited. The use of high-speed spinning disk confocal and light sheet fluorescence microscopy allows one to image the plant at single cell or even at a single organelle level. We expect future adoption of these techniques aimed at further increasing the spatio-temporal resolution of the analyses of Ca^{2+} dynamics. A high-end microscopy approach that is also used to monitor FRET-based sensors involves the measurement of fluorescent lifetimes of the donor molecule. This requires a pulsed laser, coupled to a very fast, high resolution photon counting device to determine the time of fluorescence emission of every molecule after excitation. A great advantage of this approach is that the readout is independent of expression levels and that the combination with dark acceptors allows for multiplex analysis. However, given that many photons need to be counted, there are important limitations to the speed by which the imaging can proceed. Current technologies are starting to achieve the required speed (fast-FRET-FLIM) for imaging fast processes such as Ca^{2+} signaling and will be instrumental for multiplexed imaging of a variety of sensors.

At a larger spatial scale, plants expressing two or more sensors simultaneously, with non-overlapping spectra, can be analyzed with low magnification (Resentini et al., 2021a), for example with a stereomicroscope equipped with an automatized filters wheel and multiple LED light sources. A low magnification approach is particularly well suited for imaging plants in close-to-physiological conditions. However, one must bear in mind that when dealing with large plant organs, one major limitation of optical imaging is the diffusion of light within them. Photoacoustic imaging which combines ultrasonic resolution with high contrast and specificity of light (Xu and Wang, 2006) could solve this problem. In photoacoustic imaging, short laser pulses are used to generate megahertz ultrasound waves in-depth into the tissue, usually referred to as photoacoustic, optoacoustic, or thermoacoustic signals. Dyes, GECIs, and metallochromic Ca^{2+} indicators (Dean-Ben et al., 2017; Liu et al., 2019; Dana et al., 2016; Roberts et al., 2018) have been proposed for photoacoustic imaging and imaging of the neural dynamics has been demonstrated in the mammalian brain, at depths superior to fluorescence microscopy (Gottschalk et al., 2019). Photoacoustic technology has not yet been used, to our knowledge, for volumetric Ca^{2+} imaging in plant biology. However, considering that photoacoustic imaging offers possibilities such as pigment identification (Tserevelakis et al., 2016) and chemoselective imaging (Zeng et al., 2019), it could potentially be a key technology in the years to come. The development of additional imaging technologies should allow plants to be kept in their pots without being touched or perturbed until the day of the experiment.

As a further development, additional genetic screens could be designed. As an example, the mutagenesis of plant lines expressing different GECIs in different cellular locales could be developed. The generated mutants could be screened with a fluorescent plate reader (Wagner et al., 2019) to identify those mutants impaired in the Ca^{2+} accumulation in a given compartment.

Conclusions

We are facing a revolution in terms of imaging that is based on the availability of tools that will permit us to really use this technology to increase our knowledge about how plants cope with and adapt to a changing environment. We are now getting closer to perform imaging experiments in real physiological conditions and not being limited to the use of

OUTSTANDING QUESTIONS

- Can GECIs be used for in vivo analyses of Ca^{2+} dynamics in real physiological conditions?
- Can Ca^{2+} imaging technology in model plants translate to crops?
- Can GECIs be used as environmental biosensors?
- Can we design genetic screening based on recent generation GECIs to identify additional components of Ca^{2+} signaling?

a specimen mounted on a microscope slide. Imaging technologies are non-destructive and can be used to extract information from the plants at a whole-plant resolution, from one organ or organelle to another within the same plant (Lew et al., 2020).

Supplemental data

The following materials are available in the online version of this article.

Supplemental Figure S1. Single wavelength emissions as arbitrary units of fluorescence of cpVenus (yellow trace) and ECFP (light blue trace) of the YC-Nano 65 used for the ratio calculations of Figure 3, C and G.

Acknowledgments

We thank Dr. Melanie Krebs (University of Heidelberg) for providing us the pUBQ10-R-GECO1 and pUBQ10-pH-GFP Arabidopsis lines and Prof. Joerg Kudla (University of Muenster) for providing us the pCaMV35S-YC Nano 65 Cameleon Arabidopsis line.

Funding

This work was supported by Piano di Sviluppo di Ateneo 2019 (University of Milan) (to A.C.), by a PhD fellowship from the University of Milan (to M.G.), by Ministero dell'Istruzione, dell'Università e della Ricerca Fondo per Progetti di ricerca di Rilevante Interesse Nazionale 2017 (PRIN 2017ZBBYNC) for a postdoctoral fellowship (to F.R.); by Ministero dell'Istruzione, dell'Università e della Ricerca Fondo per Progetti di ricerca di Rilevante Interesse Nazionale 2017 (PRIN 2017FBS8YN) (to M.Z.), and by a FWO Research Grant (G002220N) (to S.V.).

Conflict of interest statement. The authors have declared that no conflict of interests exist.

References

Alfieri A, Doccula FG, Pederzoli R, Grenzi M, Bonza MC, Luoni L, Candeo A, Romano Armada N, Barbiroli A, Valentini G, et al. (2020) The structural bases for agonist diversity in an *Arabidopsis thaliana* glutamate receptor-like channel. Proc Natl Acad Sci USA **117**: 752–760

Alford SC, Ding Y, Simmen T, Campbell RE (2012) Dimerization-dependent green and yellow fluorescent proteins. ACS Synth Biol **21**: 569–575

Allen DG, Blinks JR, Prendergast FG (1977) Aequorin luminescence: Relation of light emission to calcium concentration—a calcium-independent component. Science **195**: 996–998

Allen GJ, Kwak JM, Chu SP, Llopis J, Tsien RY, Harper JF, Schroeder JI (1999) Cameleon calcium indicator reports cytoplasmic calcium dynamics in Arabidopsis guard cells. Plant J **19**: 735–747

Ashrafi G, de Juan-Sanz J, Farrell RJ, Ryan TA (2020) Molecular tuning of the axonal mitochondrial Ca^{2+} uniporter ensures metabolic flexibility of neurotransmission. Neuron **105**: 678–687.e5

Ast C, Foret J, Oltrogge LM, De Michele R, Kleist TJ, Ho CH, Frommer WB (2017) Ratiometric Matryoshka biosensors from a nested cassette of green- and orange-emitting fluorescent proteins. Nat Commun **8**: 431

Baird GS, Zacharias DA, Tsien RY (1999) Circular permutation and receptor insertion within green fluorescent proteins. Proc Natl Acad Sci USA **96**: 11241–11246

Baubet V, Le Mouellic H, Campbell AK, Lucas-Meunier E, Fossier P, Brulet P (2000) Chimeric green fluorescent protein-aequorin as bioluminescent Ca^{2+} reporters at the single-cell level. Proc Natl Acad Sci USA **97**: 7260–7265

Behera S, Wang N, Zhang C, Schmitz-Thom I, Strohkamp S, Schültke S, Hashimoto K, Xiong L, Kudla J (2015) Analyses of Ca^{2+} dynamics using a ubiquitin-10 promoter-driven Yellow Cameleon 3.6 indicator reveal reliable transgene expression and differences in cytoplasmic Ca^{2+} responses in Arabidopsis and rice (*Oryza sativa*) roots. New Phytol **206**: 751–760

Behera S, Zhaolong X, Luoni L, Bonza MC, Doccula FG, De Michelis MI, Morris RJ, Schwarzländer M, Costa A (2018) Cellular Ca^{2+} signals generate defined pH signatures in plants. Plant Cell **30**: 2704–2719

Beneloujaephajri E, Costa A, L'Haridon F, Métraux JP, Binda M (2013) Production of reactive oxygen species and wound-induced resistance in *Arabidopsis thaliana* against *Botrytis cinerea* are preceded and depend on a burst of calcium. BMC Plant Biol **13**: 160

Benikhlef L, L'Haridon F, Abou-Mansour E, Serrano M, Binda M, Costa A, Lehmann S, Métraux JP (2013) Perception of soft mechanical stress in Arabidopsis leaves activates disease resistance. BMC Plant Biol 13: 133

Berridge MJ, Lipp P, Bootman MD (2000) The versatility and universality of calcium signalling. Nat Rev Mol Cell Biol **1**: 11–21

Bonza MC, Loro G, Behera S, Wong A, Kudla J, Costa A (2013) Analyses of Ca^{2+} accumulation and dynamics in the endoplasmic reticulum of Arabidopsis root cells using a genetically encoded Cameleon sensor. Plant Physiol **163**: 1230–1241

Brini M, Marsault R, Bastianutto C, Alvarez J, Pozzan T, Rizzuto R (1995) Transfected aequorin in the measurement of cytosolic Ca^{2+} concentration ($[Ca^{2+}]c$). A critical evaluation. Journal of Biological Chemistry **270**: 9896–9903

Bush DS, Jones RL (1987) Measurement of cytoplasmic calcium in aleurone protoplasts using indo-1 and fura-2. Cell Calcium **8**: 455–472

Bush DS, Jones RL (1990) Measuring intracellular Ca levels in plant cells using the fluorescent probes, indo-1 and fura-2: Progress and prospects. Plant Physiol **93**: 841–845

Candeo A, Doccula FG, Valentini G, Bassi A, Costa A (2017) Light sheet fluorescence microscopy quantifies calcium oscillations in root hairs of *Arabidopsis thaliana*. Plant Cell Physiol **58**: 1161–1172

Carafoli E, Krebs J (2016) Why calcium? How calcium became the best communicator. J Biol Chem **291**: 20849–20857

Chen K, Gao J, Sun S, Zhang Z, Yu B, Li J, Xie C, Li G, Wang P, Song C-P, et al. (2020) BONZAI proteins control global osmotic stress responses in plants. Current Biol **30**: 4815–4825

Chen TW, Wardill TJ, Sun Y, Pulver SR, Renninger SL, Baohan A, Schreiter ER, Kerr RA, Orger MB, Jayaraman V, et al. (2013) Ultrasensitive fluorescent proteins for imaging neuronal activity. Nature **499**: 295–300

Choi WG, Toyota M, Kim SH, Hilleary R, Gilroy S (2014) Salt stress-induced Ca^{2+} waves are associated with rapid, long-distance root-to-shoot signaling in plants. Proc Natl Acad Sci USA **111**: 6497–6502

Clapham DE (2007) Calcium signaling. Cell **14**: 1047–1058

Corso M, Doccula FG, de Melo JRF, Costa A, Verbruggen N (2018) Endoplasmic reticulum-localized CCX2 is required for osmotolerance by regulating ER and cytosolic Ca^{2+} dynamics in Arabidopsis. Proc Natl Acad Sci USA **115**: 3966–3971

Costa A, Candeo A, Fieramonti L, Valentini G, Bassi A (2013) Calcium dynamics in root cells of *Arabidopsis thaliana* visualized with selective plane illumination microscopy. PLoS ONE **8**: e75646

Costa A, Drago I, Behera S, Zottini M, Pizzo P, Schroeder JI, Pozzan T, Lo Schiavo F (2010) H_2O_2 in plant peroxisomes: an in vivo analysis uncovers a Ca^{2+}-dependent scavenging system. Plant J **62**: 760–772

Costa A, Luoni L, Marrano CA, Hashimoto K, Köster P, Giacometti S, De Michelis MI, Kudla J, Bonza MC (2017) Ca^{2+}-dependent phosphoregulation of the plasma membrane Ca^{2+}-ATPase ACA8 modulates stimulus-induced calcium signatures. J Exp Bot **68**: 3215–3230

Costa A, Navazio L, Szabo I (2018) The contribution of organelles to plant intracellular calcium signalling. J Exp Bot **69**: 4175–4193

Dana H, Mohar B, Sun Y, Narayan S, Gordus A, Hasseman JP, Tsegaye G, Holt GT, Hu A, Walpita D, et al. (2016) Sensitive red protein calcium indicators for imaging neural activity. eLife 5: e12727

Dana H, Sun Y, Mohar B, Hulse BK, Kerlin AM, Hasseman JP, Tsegaye G, Tsang A, Wong A, Patel R, et al. (2019) High-performance calcium sensors for imaging activity in neuronal populations and microcompartments. Nat Methods **16**: 649–657

Dana N, Fowler RA, Allen A, Zoldan J, Suggs L, Emelianov S (2016) *In vitro* photoacoustic sensing of calcium dynamics with arsenazo III. Laser Phys Lett **13**: 075603.

de Juan-Sanz J, Holt GT, Schreiter ER, de Juan F, Kim DS, Ryan TA (2017) Axonal endoplasmic reticulum Ca^{2+} content controls release probability in CNS nerve terminals. Neuron **93**: 867–881.e6.

Dean-Ben XL, Gottschalk S, Sela G, Shoham S, Razansky D (2017) Functional optoacoustic neuro-tomography of calcium fluxes in adult zebrafish brain in vivo. Opt Lett **42**: 959–962

DeFalco TA, Bender KW, Snedden WA (2010) Breaking the code: Ca^{2+} sensors in plant signalling. Biochem J **425**: 27–40

DeFalco TA, Toyota M, Phan V, Karia P, Moeder W, Gilroy S, Yoshioka K (2017) Using GCaMP3 to study Ca^{2+} signaling in Nicotiana species. Plant Cell Physiol **58**: 1173–1184

Demidchik V, Shabala S, Isayenkov S, Cuin TA, Pottosin I (2018) Calcium transport across plant membranes: Mechanisms and functions. New Phytol **220**: 49–69

Denninger P, Bleckmann A, Lausser A, Vogler F, Ott T, Ehrhardt DW, Frommer WB, Sprunck S, Dresselhaus T, Grossmann G (2014) Male–female communication triggers calcium signatures during fertilization in Arabidopsis. Nat Commun 5: 4645

Diao M, Qu X, Huang S (2018) Calcium imaging in Arabidopsis pollen cells using G-CaMP5. J Integr Plant Biol **60**: 897–906

Dindas J, Scherzer S, Roelfsema MRG, von Meyer K, Müller HM, Al-Rasheid KAS, Palme K, Dietrich P, Becker D, Bennett MJ, et al. (2018) AUX1-mediated root hair auxin influx governs SCFTIR1/AFB-type Ca^{2+} signaling. Nat Commun **9**: 1174

Doccula FG, Luoni L, Behera S, Bonza MC, Costa A (2018) In vivo analysis of calcium levels and glutathione redox status in Arabidopsis epidermal leaf cells infected with the hypersensitive response-inducing bacteria *Pseudomonas syringae* pv. tomato AvrB (PstAvrB). Methods Mol Biol **1743**: 125–141

Dodd AN, Jakobsen MK, Baker AJ, Telzerow A, Hou SW, Laplaze L, Barrot L, Poethig RS, Haseloff J, Webb AA (2006) Time of day modulates low-temperature Ca signals in Arabidopsis. Plant J **48**: 962–973

Edel KH, Marchadier E, Brownlee C, Kudla J, Hetherington AM (2017) The evolution of calcium-based signalling in plants. Curr Biol **27**: R667–R679

Ehrhardt DW, Wais R, Long SR (1996) Calcium spiking in plant root hairs responding to Rhizobium nodulation signals. Cell **85**: 673–681

Fasani E, DalCorso G, Costa A, Zenoni S, Furini A. (2019) The *Arabidopsis thaliana* transcription factor MYB59 regulates calcium signalling during plant growth and stress response. Plant Mol Biol **99**: 517–534

Fichman Y, Mittler R (2021) Integration of electric, calcium, reactive oxygen species and hydraulic signals during rapid systemic signaling in plants. Plant J (doi:10.1111/tpj.15360)

Gao D, Knight MR, Trewavas AJ, Sattelmacher B, Plieth C (2004) Self-reporting Arabidopsis expressing pH and [Ca^{2+}] indicators unveil ion dynamics in the cytoplasm and in the apoplast under abiotic stress. Plant Physiol **134**: 898–908

Garcia-Mata C, Gay R, Sokolovski S, Hills A, Lamattina L, Blatt MR (2003) Nitric oxide regulates K^+ and Cl^- channels in guard cells through a subset of abscisic acid-evoked signaling pathways. Proc Natl Acad Sci USA **100**: 11116–111121

Gilroy S, Fricker MD, Read ND, Trewavas AJ (1991) Role of calcium in signal transduction of Commelina guard cells. Plant Cell **3**: 333–344

Goedhart J, van Weeren L, Hink MA, Vischer NO, Jalink K, Gadella TW Jr (2010) Bright cyan fluorescent protein variants identified by fluorescence lifetime screening. Nat Methods **7**: 137–139

Gottschalk S, Degtyaruk O, McLarney B, Rebling J, Hutter MA, Deán-Ben XL, Shoham S, Razansky D (2019) Rapid volumetric optoacoustic imaging of neural dynamics across the mouse brain. Nat Biomed Eng **3**: 392–401

Greenwald EC, Mehta S, Zhang J (2018) Genetically encoded fluorescent biosensors illuminate the spatiotemporal regulation of signaling networks. Chem Rev **118**: 11707–11794

Grefen C, Donald N, Hashimoto K, Kudla J, Schumacher K, Blatt MR (2010) A ubiquitin-10 promoter-based vector set for fluorescent protein tagging facilitates temporal stability and native protein distribution in transient and stable expression studies. Plant J **64**: 355–365

Hamamura Y, Nishimaki M, Takeuchi H, Geitmann A, Kurihara D, Higashiyama T (2014) Live imaging of calcium spikes during double fertilization in Arabidopsis. Nat Commun **5**: 4722

Hazak O, Mamon E, Lavy M, Sternberg H, Behera S, Schmitz-Thom I, Bloch D, Dementiev O, Gutman I, Danziger T, et al. (2019) A novel Ca^{2+}-binding protein that can rapidly transduce auxin responses during root growth. PLoS Biol **17**: e3000085

Hedrich R, Neher E (2018) Venus flytrap: how an excitable, carnivorous plant works. Trends Plant Sci **23**: 220–234 PMID: 29336976 DOI: 10.1016/j.tplants.2017.12.004

Heim N, Garaschuk O, Friedrich MW, Mank M, Milos RI, Kovalchuk Y, Konnerth A, Griesbeck O (2007) Improved calcium imaging in transgenic mice expressing a troponin C-based biosensor. Nat Methods **4**: 127–129

Hilleary R, Paez-Valencia J, Vens C, Toyota M, Palmgren M, Gilroy S (2020) Tonoplast-localized Ca^{2+} pumps regulate Ca^{2+} signals during pattern-triggered immunity in *Arabidopsis thaliana*. Proc Natl Acad Sci USA **117**: 18849–18857

Holdaway-Clarke TL, Feijo JA, Hackett GR, Kunkel JG, Hepler PK (1997) Pollen tube growth and the intracellular cytosolic calcium gradient oscillate in phase while extracellular calcium influx is delayed. Plant Cell **9**: 1999–2010

Horikawa K, Yamada Y, Matsuda T, Kobayashi K, Hashimoto M, Matsu-ura T, Miyawaki A, Michikawa T, Mikoshiba K, Nagai T

(2010) Spontaneous network activity visualized by ultrasensitive Ca^{2+} indicators, yellow Cameleon-Nano. Nat Methods **7**: 729–732

Ishka MR, Brown E, Rosenberg A, Romanowsky S, Davis J, Choi W-G, Harper JF (2021) Arabidopsis Ca^{2+}-ATPases 1, 2, and 7 in the endoplasmic reticulum contribute to growth and pollen fitness. Plant Phys **185**: 1966–1985

Iwano M, Entani T, Shiba H, Kakita M, Nagai T, Mizuno H, Miyawaki A, Shoji T, Kubo K, Isogai A, et al. (2009) Fine-tuning of the cytoplasmic Ca^{2+} concentration is essential for pollen tube growth. Plant Physiol **150**: 1322–1334

Jiang Z, Zhou X, Tao M, Yuan F, Liu L, Wu F, Wu X, Xiang Y, Niu Y, Liu F, et al. (2019) Plant cell-surface GIPC sphingolipids sense salt to trigger Ca^{2+} influx. Nature **572**: 341–346

Johnson CH, Knight MR, Kondo T, Masson P, Sedbrook J, Haley A, Trewavas A (1995) Circadian oscillations of cytosolic and chloroplastic free calcium in plants. Science **269**: 1863–1865

Keinath NF, Waadt R, Brugman R, Schroeder JI, Grossmann G, Schumacher K, Krebs M (2015) Live cell imaging with R-GECO1 sheds light on flg22- and chitin-induced transient $[Ca^{2+}]_{cyt}$ patterns in Arabidopsis. Mol Plant **8**: 1188–1200

Kelner A, Leitao N, Chabaud M, Charpentier M, de Carvalho-Niebel F (2018) Dual color sensors for simultaneous analysis of calcium signal dynamics in the nuclear and cytoplasmic compartments of plant cells. Front Plant Sci **9**: 245

Kiegle E, Moore CA, Haseloff J, Tester MA, Knight MR (2000) Cell-type-specific calcium responses to drought, salt and cold in the Arabidopsis root. Plant J **23**: 267–278

Kiep V, Vadassery J, Lattke J, Maass JP, Boland W, Peiter E, Mithofer A (2015) Systemic cytosolic Ca^{2+} elevation is activated upon wounding and herbivory in Arabidopsis. New Phytol **207**: 996–1004

Kleist TJ, Cartwright HN, Perera AM, Christianson ML, Lemaux PG, Luan S (2017) Genetically encoded calcium indicators for fluorescence imaging in the moss *Physcomitrella*: GCaMP3 provides a bright new look. Plant Biotechnol J **15**: 1235–1237

Klejchova M, Silva-Alvim FAL, Blatt MR, Alvim JC (2021) Membrane voltage as a dynamic platform for spatio-temporal signalling, physiological and developmental regulation. Plant Physiol **185**: 1523–1541

Knight H, Trewavas AJ, Knight MR (1996) Cold calcium signaling in Arabidopsis involves two cellular pools and a change in calcium signature after acclimation. Plant Cell **8**: 489–503

Knight MR, Campbell AK, Smith SM, Trewavas AJ (1991) Transgenic plant aequorin reports the effects of touch and cold-shock and elicitors on cytoplasmic calcium. Nature **352**: 524–526

Komis G, Šamajová O, Ovečka M, Šamaj J (2015) Super-resolution microscopy in plant cell imaging. Trends Plant Sci **20**: 834–843.

Krebs M, Held K, Binder A, Hashimoto K, Den Herder G, Parniske M, Kudla J, Schumacher K (2012) FRET-based genetically encoded sensors allow high-resolution live cell imaging of Ca^{2+} dynamics. Plant J **69**: 181–192

Krebs M, Schumacher K (2013) Live cell imaging of cytoplasmic and nuclear Ca^{2+} dynamics in Arabidopsis roots. Cold Spring Harb Protoc 2013: 776–780

Krogman W, Sparks JA, Blancaflor EB (2020) Cell type-specific imaging of calcium signaling in *Arabidopsis thaliana* seedling roots using GCaMP3. Int J Mol Sci **21**: 6385

Kudla J, Batistic O, Hashimoto K (2010) Calcium signals: the lead currency of plant information processing. Plant Cell **22**: 541–563

Kudla J, Becker D, Grill E, Hedrich R, Hippler M, Kummer U, Parniske M, Romeis T, Schumacher K (2018) Advances and current challenges in calcium signaling. New Phytol **218**: 414–431

Laanemets K, Wang YF, Lindgren O, Wu J, Nishimura N, Lee S, Caddell D, Merilo E, Brosche M, Kilk K, et al. (2013) Mutations in the SLAC1 anion channel slow stomatal opening and severely reduce K^+ uptake channel activity via enhanced cytosolic $[Ca^{2+}]$ and increased Ca^{2+} sensitivity of K^+ uptake channels. New Phytol **197**: 88–98

Laissue PP, Alghamdi RA, Tomancak P, Reynaud EG, Shroff H (2017) Assessing phototoxicity in live fluorescence imaging. Nat Methods **14**: 657–661

Leitão N, Dangeville P, Carter R, Charpentier M (2019) Nuclear calcium signatures are associated with root development. Nat Commun **10**: 4865

Lenglet A, Jaslan D, Toyota M, Mueller M, Muller T, Schonknecht G, Marten I, Gilroy S, Hedrich R, Farmer EE (2017) Control of basal jasmonate signalling and defence through modulation of intracellular cation flux capacity. New Phytol **216**: 1161–1169

Lew TTS, Sarojam R, Jang IC, Park BS, Naqvi NI, Wong MH, Singh GP, Ram RJ, Shoseyov O, Saito K, et al. (2020) Species-independent analytical tools for next-generation agriculture. Nat Plants **6**: 1408–1417

Li K, Prada J, Damineli DSC, Liese A, Romeis T, Dandekar T, Feijó JA, Hedrich R, Konrad KR (2021) An optimized genetically encoded dual reporter for simultaneous ratio imaging of Ca^{2+} and H^+ reveals new insights into ion signaling in plants. New Phytol (doi:10.1111/nph.17202)

Liu KH, Niu Y, Konishi M, Wu Y, Du H, Sun Chung H, Li L, Boudsocq M, McCormack M, Maekawa S, et al. (2017) Discovery of nitrate-CPK-NLP signalling in central nutrient-growth networks. Nature **545**: 311–316

Liu WW, Chen SH, Li PC (2019) Functional calcium imaging using optical-resolution photoacoustic microscopy in a 3D tumor cell culture. Proc SPIE (https://doi.org/10.1117/12.2510936)

Logan DC, Knight MR (2003) Mitochondrial and cytosolic calcium dynamics are differentially regulated in plants. Plant Physiol **133**: 21–24

Loro G, Costa A (2013) Imaging of mitochondrial and nuclear Ca^{2+} dynamics in Arabidopsis roots. Cold Spring Harb Protoc **8**: 781–785

Loro G, Drago I, Pozzan T, Schiavo FL, Zottini M, Costa A (2012) Targeting of Cameleons to various subcellular compartments reveals a strict cytoplasmic/mitochondrial Ca^{2+} handling relationship in plant cells. Plant J **71**: 1–13

Loro G, Wagner S, Doccula FG, Behera S, Weinl S, Kudla J, Schwarzlander M, Costa A, Zottini M (2016) Chloroplast-specific in vivo Ca^{2+} imaging using Yellow Cameleon fluorescent protein sensors reveals organelle-autonomous Ca^{2+} signatures in the stroma. Plant Physiol **171**: 2317–2330

Love J, Dodd AN, Webb AA (2004) Circadian and diurnal calcium oscillations encode photoperiodic information in Arabidopsis. Plant Cell **16**: 956–966

Luo J, Chen L, Huang F, Gao P, Zhao H, Wang Y, Han S (2020) Intraorganellar calcium imaging in Arabidopsis seedling roots using the GCaMP variants GCaMP6m and R-CEPIA1er. J Plant Physiol **246–247**: 153127

Martí MC, Stancombe MA, Webb AA (2013) Cell- and stimulus type-specific intracellular free Ca^{2+} signals in Arabidopsis. Plant Physiol **163**: 625–634

Martí Ruiz MC, Jung HJ, Webb AAR (2020) Circadian gating of dark-induced increases in chloroplast- and cytosolic-free calcium in Arabidopsis. New Phytol **225**: 1993–2005

McAinsh MR, Brownlee C, Hetherington AM (1990) Abscisic acid-induced elevation of guard cell cytosolic Ca^{2+} precedes stomatal closure. Nature **343**: 186–188

McAinsh MR, Pittman JK (2009) Shaping the calcium signature. New Phytol **181**: 275–294

McAinsh MR, Webb A, Taylor JE, Hetherington AM (1995) Stimulus-induced oscillations in guard cell cytosolic free calcium. Plant Cell **7**: 1207–1219

Mehlmer N, Parvin N, Hurst CH, Knight MR, Teige M, Vothknecht UC (2012) A toolset of aequorin expression vectors for in planta studies of subcellular calcium concentrations in *Arabidopsis thaliana*. J Exp Bot **63**: 1751–1761

Mehta S, Zhang Y, Roth RH, Zhang JF, Mo A, Tenner B, Huganir RL, Zhang J (2018) Single-fluorophore biosensors for sensitive and multiplexed detection of signalling activities. Nat Cell Biol **20**: 1215–1225

Michard E, Dias P, Feijó JA (2008) Tobacco pollen tubes as cellular models for ion dynamics: improved spatial and temporal resolution of extracellular flux and free cytosolic concentration of calcium and protons using pHluorin and YC3.1 CaMeleon. Sex Plant Reprod **21**: 169–181

Michard E, Lima PT, Borges F, Silva AC, Portes MT, Carvalho JE, Gilliham M, Liu L-H, Obermeyer G, Feijó JA (2011) Glutamate receptor-like genes form Ca^{2+} channels in pollen tubes and are regulated by pistil D-serine. Science **332**: 434–437

Mithöfer A, Mazars C (2002) Aequorin-based measurements of intracellular Ca^{2+}-signatures in plant cells. Biol Proc Online **4**: 105–118

Miyawaki A, Griesbeck O, Heim R, Tsien RY (1999) Dynamic and quantitative Ca^{2+} measurements using improved Cameleons. Proc Natl Acad Sci USA **96**: 2135–2140

Miyawaki A, Llopis J, Heim R, McCaffery JM, Adams JA, Ikura M, Tsien RY (1997). Fluorescent indicators for Ca^{2+} based on green fluorescent proteins and calmodulin. Nature **388**: 882–887

Monshausen GB, Messerli MA, Gilroy S (2008) Imaging of the Yellow Cameleon 3.6 indicator reveals that elevations in cytosolic Ca^{2+} follow oscillating increases in growth in root hairs of Arabidopsis. Plant Physiol **147**: 1690–1698

Mori IC, Murata Y, Yang Y, Munemasa S, Wang YF, Andreoli S, Tiriac H, Alonso JM, Harper JF, Ecker JR, et al. (2006) CDPKs CPK6 and CPK3 function in ABA regulation of guard cell S-type anion- and Ca^{2+}-permeable channels and stomatal closure. PLoS Biol **4**: e327

Moseyko N, Feldman LJ (2001) Expression of pH-sensitive green fluorescent protein in *Arabidopsis thaliana*. Plant Cell Environ **24**: 557–563

Nagai T, Ibata K, Park ES, Kubota M, Mikoshiba K, Miyawaki A (2002) A variant of yellow fluorescent protein with fast and efficient maturation for cell-biological applications. Nat Biotechnol **20**: 87–90

Nagai T, Yamada S, Tominaga T, Ichikawa M, Miyawaki A (2004) Expanded dynamic range of fluorescent indicators for Ca^{2+} by circularly permuted yellow fluorescent proteins. Proc Natl Acad Sci USA **101**: 10554–10559

Nakai J, Ohkura M, Imoto K (2001) A high signal-to-noise Ca^{2+} probe composed of a single green fluorescent protein. Nat Biotechnol **19**: 137–141

Ngo QA, Vogler H, Lituiev DS, Nestorova A, Grossniklaus U (2014) A calcium dialog mediated by the FERONIA signal transduction pathway controls plant sperm delivery. Dev Cell **29**: 491–500

Nguyen CT, Kurenda A, Stolz S, Chételat A, Farmer EE (2018) Identification of cell populations necessary for leaf-to-leaf electrical signaling in a wounded plant. Proc Natl Acad Sci USA **115**: 10178–10183

Ohmiya Y, Hirano T (1996) Shining the light: The mechanism of the bioluminescence reaction of calcium-binding photoproteins. Chem Biol **3**: 337–347

Ordenes VR, Moreno I, Maturana D, Norambuena L, Trewavas AJ, Orellana A (2012) *In vivo* analysis of the calcium signature in the plant Golgi apparatus reveals unique dynamics. Cell Calcium **52**: 397–404

Palmer AE, Giacomello M, Kortemme T, Hires SA, Lev-Ram V, Baker D, Tsien RY (2006) Ca^{2+} indicators based on computationally redesigned calmodulin-peptide pairs. Chem Biol **13**: 521–530

Palmer AE, Jin C, Reed JC, Tsien RY (2004) Bcl-2-mediated alterations in endoplasmic reticulum Ca^{2+} analyzed with an improved genetically encoded fluorescent sensor. Proc Natl Acad Sci USA **101**: 17404–17409

Palmer AE, Tsien RY (2006) Measuring calcium signaling using genetically targetable fluorescent indicators. Nat Protoc **1**: 1057–1065

Palmgren MG (2001) PLANT PLASMA MEMBRANE H^+-ATPases: powerhouses for nutrient uptake. Annu Rev Plant Physiol Plant Mol Biol **52**: 817–845

Peragine A, Yoshikawa M, Wu G, Albrecht HL, Poethig RS (2004) SGS3 and SGS2/SDE1/RDR6 are required for juvenile development and the production of trans-acting siRNAs in Arabidopsis. Genes Dev **18**: 2368–2379

Perez Koldenkova V, Nagai T (2013) Genetically encoded Ca^{2+} indicators: properties and evaluation. Biochim Biophys Acta **1833**: 1787–1797

Pirayesh N, Giridhar M, Ben Khedher A, Vothknecht UC, Chigri F (2021) Organellar calcium signaling in plants: An update. Biochim Biophys Acta Mol Cell Res **1868**: 118948

Prasher D, McCann RO, Cormier MJ (1985) Cloning and expression of the cDNA coding for aequorin, a bioluminescent calcium-binding protein. Biochem Biophys Res Commun **126**: 1259–1268

Prasher DC, Eckenrode VK, Ward WW, Prendergast FG, Cormier MJ (1992) Primary structure of the *Aequorea victoria* green-fluorescent protein. Gene **111**: 229–233

Resentini F, Grenzi M, Ancora D, Cademartori M, Luoni L, Franco M, Bassi A, Bonza MC, Costa A (2021a) Simultaneous imaging of ER and cytosolic Ca^{2+} dynamics reveals long-distance ER Ca^{2+} waves in plants. Plant Physiol **187**: 603–617

Resentini F, Ruberti C, Grenzi M, Bonza MC, Costa A (2021b) The signatures of organellar calcium. Plant Physiol (doi.org/10.1093/plphys/kiab189)

Robert V, Pinton P, Tosello V, Rizzuto R, Pozzan T (2000) Recombinant aequorin as tool for monitoring calcium concentration in subcellular compartments. Methods Enzymol **327**: 440–456

Roberts S, Seeger M, Jiang Y, Mishra A, Sigmund F, Stelzl A, Lauri A, Symvoulidis P, Rolbieski H, Preller M, et al. (2018) Calcium sensor for photoacoustic imaging. J Am Chem Soc **140**: 2718–2721

Rogers KL, Stinnakre J, Agulhon C, Jublot D, Shorte SL, Kremer EJ, Brulet P (2005) Visualization of local Ca^{2+} dynamics with genetically encoded bioluminescent reporters. Eur J Neurosci **21**: 597–610

Romano Armada N, Doccula FG, Candeo A, Valentini G, Costa A, Bassi A (2019) *In vivo* light sheet fluorescence microscopy of calcium oscillations in *Arabidopsis thaliana*. Methods Mol Biol **1925**: 87–101

Rudolf R, Mongillo M, Rizzuto R, Pozzan T (2003) Looking forward to seeing calcium. Nat Rev Mol Cell Biol **4**: 579–586

Sai J, Johnson CH (2002) Dark-stimulated calcium ion fluxes in the chloroplast stroma and cytosol. Plant Cell **14**: 1279–1291

Sanders D, Pelloux J, Brownlee C, Harper JF (2002) Calcium at the crossroads of signaling. Plant Cell 14: S401–S417

Scherzer S, Böhm J, Krol E, Shabala L, Kreuzer I, Larisch C, Bemm F, Al-Rasheid KA, Shabala S, Rennenberg H, et al. (2015) Calcium sensor kinase activates potassium uptake systems in gland cells of Venus flytraps. Proc Natl Acad Sci USA **112**: 7309–7314

Sello S, Moscatiello R, Mehlmer N, Leonardelli M, Carraretto L, Cortese E, Zanella FG, Baldan B, Szabo I, Vothknecht UC, et al. (2018) Chloroplast Ca^{2+} fluxes into and across thylakoids revealed by thylakoid-targeted aequorin probes. Plant Physiol **177**: 38–51

Sello S, Perotto J, Carraretto L, Szabo I, Vothknecht UC, Navazio L (2016) Dissecting stimulus-specific Ca^{2+} signals in amyloplasts and chloroplasts of *Arabidopsis thaliana* cell suspension cultures. J Exp Bot **67**: 3965–3974

Shao Q, Gao Q, Lhamo D, Zhang H, Luan S (2020) Two glutamate- and pH-regulated Ca^{2+} channels are required for systemic wound signaling in Arabidopsis. Sci Signal **13**: eaba1453

Shaw SL, Thoms D, Powers J (2019) Structured illumination approaches for super-resolution in plant cells. Microscopy **68**: 37–44

Shen Y, Dana H, Abdelfattah AS, Patel R, Shea J, Molina RS, Rawal B, Rancic V, Chang YF, Wu L, et al. (2018) A genetically encoded Ca^{2+} indicator based on circularly permutated sea anemone red fluorescent protein eqFP578. BMC Biol **16**: 9

Shimomura O (1995) A short story of aequorin. Biol Bull **189**: 1–5

Shimomura O, Johnson FH, Saiga Y (1962) Extraction, purification and properties of aequorin, a bioluminescent protein from the luminous hydromedusan, *Aequorea*. J Cell Comp Physiol **59**: 223–239

Shkolnik D, Nuriel R, Bonza MC, Costa A, Fromm H (2018) MIZ1 regulates ECA1 to generate a slow, long-distance phloem-transmitted Ca^{2+} signal essential for root water tracking in Arabidopsis. Proc Natl Acad Sci USA **115**: 8031–8036

Souslova EA, Belousov VV, Lock JG, Strömblad S, Kasparov S, Bolshakov AP, Pinelis VG, Labas YA, Lukyanov S, Mayr LM, et al. (2007) Single fluorescent protein-based $Ca2^{+}$ sensors with increased dynamic range. BMC Biotechnol. 29;**7**:37

Stael S, Wurzinger B, Mair A, Mehlmer N, Vothknecht UC, Teige M (2012) Plant organellar calcium signalling: an emerging field. J Exp Bot **63**: 1525–1542

Storti M, Costa A, Golin S, Zottini M, Morosinotto T, Alboresi A (2018) Systemic calcium wave propagation in *Physcomitrella patens*. Plant Cell Physiol **59**: 1377–1384

Suda H, Mano H, Toyota M, Fukushima K, Mimura T, Tsutsui I, Hedrich R, Tamada Y, Hasebe M (2020) Calcium dynamics during trap closure visualized in transgenic Venus flytrap. Nat Plants **6**: 1219–1224

Suzuki J, Kanemaru K, Ishii K, Ohkura M, Okubo Y, Iino M (2014) Imaging intraorganellar Ca^{2+} at subcellular resolution using CEPIA. Nat Commun 5: 4153

Taiz L, Zeiger E, Møller IM, Murphy A (2014) Plant Physiology and Development. Ed 6, Sinauer Associates Inc., Sunderland, Massachusetts, USA. ISBN: 9781605352558

Tanaka K, Swanson SJ, Gilroy S, Stacey G (2010) Extracellular nucleotides elicit cytosolic free calcium oscillations in Arabidopsis. Plant Physiol **154**: 705–719

Teardo E, Carraretto L, Wagner S, Formentin E, Behera S, De Bortoli S, Larosa V, Fuchs P, Lo Schiavo F, Raffaello A, et al. (2017) Physiological characterization of a plant mitochondrial calcium uniporter *in vitro* and *in vivo*. Plant Physiol **173**: 1355–1370

Thestrup T, Litzlbauer J, Bartholomäus I, Mues M, Russo L, Dana H, Kovalchuk Y, Liang Y, Kalamakis G, Laukat Y, et al. (2014) Optimized ratiometric calcium sensors for functional in vivo imaging of neurons and T lymphocytes. Nat Methods **11**: 175–182

Tian L, Hires SA, Mao T, Huber D, Chiappe ME, Chalasani SH, Petreanu L, Akerboom J, McKinney SA, Schreiter ER, et al. (2009) Imaging neural activity in worms, flies and mice with improved GCaMP calcium indicators. Nat Methods **6**: 875–881

Tian W, Wang C, Gao Q, Li L, Luan S. (2020) Calcium spikes, waves and oscillations in plant development and biotic interactions. Nat Plants **6**: 750–759

Toyota M, Spencer D, Sawai-Toyota S, Jiaqi W, Zhang T, Koo AJ, Howe GA, Gilroy S (2018) Glutamate triggers long-distance, calcium-based plant defense signaling. Science **361**: 1112–1115

Tserevelakis GJ, Tsagkaraki M, Zacharakis G (2016) Hybrid photoacoustic and optical imaging of pigments in vegetative tissues. J Microsc **263**: 300–306

Tsien RY (1980) New calcium indicators and buffers with high selectivity against magnesium and protons: design, synthesis, and properties of prototype structures. Biochemistry **27**: 2396–2404

van Der Luit AH, Olivari C, Haley A, Knight MR, Trewavas AJ (1999) Distinct calcium signaling pathways regulate calmodulin gene expression in tobacco. Plant Physiol **121**: 705–714

Vincent TR, Avramova M, Canham J, Higgins P, Bilkey N, Mugford ST, Pitino M, Toyota M, Gilroy S, Miller AJ, et al. (2017) Interplay of plasma membrane and vacuolar ion channels, together with BAK1, elicits rapid cytosolic calcium elevations in Arabidopsis during aphid feeding. Plant Cell **29**: 1460–1479

Waadt R, Köster P, Andrés Z, Waadt C, Bradamante G, Lampou K, Kudla J, Schumacher K (2020) Dual-reporting transcriptionally linked genetically encoded fluorescent indicators resolve the spatiotemporal coordination of cytosolic abscisic acid and second messenger dynamics in Arabidopsis. Plant Cell **32**: 2582–2601

Waadt R, Krebs M, Kudla J, Schumacher K (2017) Multiparameter imaging of calcium and abscisic acid and high-resolution quantitative calcium measurements using R-GECO1-mTurquoise in Arabidopsis. New Phytol **216**: 303–320

Wagner S, Behera S, De Bortoli S, Logan DC, Fuchs P, Carraretto L, Teardo E, Cendron L, Nietzel T, Fussl M, et al. (2015) The EF-hand Ca^{2+} binding protein MICU choreographs mitochondrial Ca^{2+} dynamics in Arabidopsis. Plant Cell **27**: 3190–3212

Wagner S, Steinbeck J, Fuchs P, Lichtenauer S, Elsässer M, Schippers JHM, Nietzel T, Ruberti C, Van Aken O, Meyer AJ, et al. (2019) Multiparametric real-time sensing of cytosolic physiology links hypoxia responses to mitochondrial electron transport. New Phytol **224**: 1668–1684

Wang R, Himschoot E, Grenzi M, Chen J, Krebs M, Schumacher K, Nowack MK, Van Damme D, De Smet I, Beeckman T, et al. (2020) Pharmacological and genetic manipulations of Ca^{2+} signaling have contrasting effects on auxin-regulated trafficking. bioRxiv 2020.09.04.283101 (doi: https://doi.org/10.1101/2020.09.04.283101)

White PJ, Broadley MR (2003) Calcium in plants. Ann Bot **92**: 487–511

Williamson RE, Ashley CC (1982) Free Ca^{2+} and cytoplasmic streaming in the alga Chara. Nature **296**: 647–650

Wu F, Chi Y, Jiang Z, Xu Y, Xie L, Huang F, Wan D, Ni J, Yuan F, Wu X, et al. (2020) Hydrogen peroxide sensor HPCA1 is an LRR receptor kinase in Arabidopsis. Nature **578**: 577–581

Wu J, Abdelfattah AS, Miraucourt LS, Kutsarova E, Ruangkittisakul A, Zhou H, Ballanyi K, Wicks G, Drobizhev M, Rebane A, et al. (2014) A long Stokes shift red fluorescent Ca^{2+} indicator protein for two-photon and ratiometric imaging. Nat Commun **5**: 5262

Wu J, Liu L, Matsuda T, Zhao Y, Rebane A, Drobizhev M, Chang YF, Araki S, Arai Y, March K, et al. (2013) Improved orange and red Ca^{+} indicators and photophysical considerations for optogenetic applications. ACS Chem Neurosci **4**: 963–972

Xiong TC, Ronzier E, Sanchez F, Corratge-Faillie C, Mazars C, Thibaud JB (2014) Imaging long distance propagating calcium signals in intact plant leaves with the BRET-based GFP-aequorin reporter. Front Plant Sci **5**: 43

Xu M, Wang LV (2006) Photoacoustic imaging in biomedicine. Rev Sci Instrum **77**: 041101

Yang DL, Shi Z, Bao Y, Yan J, Yang Z, Yu H, Li Y, Gou M, Wang S, Zou B, et al. (2017) Calcium pumps and interacting BON1 protein modulate calcium signature, stomatal closure, and plant immunity. Plant Physiol **175**: 424–437

Yang Y, Costa A, Leonhardt N, Siegel RS, Schroeder JI (2008) Isolation of a strong Arabidopsis guard cell promoter and its potential as a research tool. Plant Methods **4**: 6

Yuan F, Yang H, Xue Y, Kong D, Ye R, Li C, Zhang J, Theprungsirikul L, Shrift T, Krichilsky B, et al. (2014) OSCA1 mediates osmotic-stress-evoked Ca^{2+} increases vital for osmosensing in Arabidopsis. Nature **514**: 367–371

Zeng L, Ma G, Xu H, Mu J, Li F, Gao X, Deng Z, Qu J, Huang P, Lin J (2019) *In vivo* chemoselective photoacoustic imaging of

copper(II) in plant and animal subjects. Small **15**: e1803866 [Is the journal title adequate?]

Zhao X, Wang YL, Qiao XR, Wang J, Wang LD, Xu CS, Zhang X (2013) Phototropins function in high-intensity blue light-induced hypocotyl phototropism in Arabidopsis by altering cytosolic calcium. Plant Physiol **162**: 1539–15351

Zhao Y, Araki S, Wu J, Teramoto T, Chang YF, Nakano M, Abdelfattah AS, Fujiwara M, Ishihara T, Nagai T, et al. (2011) An expanded palette of genetically encoded Ca^{2+} indicators. Science **333**: 1888–1891

Zhu X, Feng Y, Liang G, Liu N, Zhu JK (2013) Aequorin-based luminescence imaging reveals stimulus- and tissue-specific Ca^{2+} dynamics in Arabidopsis plants. Mol Plant **6**: 444–455

Zottini M, Zannoni D (1993) The use of fura-2 fluorescence to monitor the movement of free calcium ions into the matrix of plant mitochondria (*Pisum sativum* and *Helianthus tuberosus*). Plant Physiol **102**: 573–578